

1 **Relative terrestrial exposure ages inferred from Relationship**
2 **between meteoric ^{10}Be and NO_3^- concentrations in soils along the**
3 **Shackleton Glacier, Antarctica**

4 Melisa A. Diaz^{1,2†}, Lee B. Corbett³, Paul R. Bierman³, Byron J. Adams⁴, Diana H. Wall⁵, Ian D. Hogg^{6,7}, Noah
5 Fierer⁸, W. Berry Lyons^{1,2}

6 ¹School of Earth Sciences, The Ohio State University, Columbus, OH, 43210, USA

7 ²Byrd Polar and Climate Research Center, The Ohio State University, Columbus, OH, 43210, USA

8 ³Department of Geology, University of Vermont, Burlington, VT, 05405, USA

9 ⁴Department of Biology, Evolutionary Ecology Laboratories, and Monte L. Bean Museum, Brigham Young
10 University, Provo, UT, 84602, USA

11 ⁵Department of Biology and School of Global Environmental Sustainability, Colorado State University, Fort
12 Collins, CO, 80523, USA

13 ⁶Canadian High Arctic Research Station, Polar Knowledge Canada, Cambridge Bay, NU, X0B0C0, Canada

14 ⁷School of Science, University of Waikato, Hamilton, 3216, New Zealand

15 ⁸Department of Ecology and Evolutionary Biology and Cooperative Institute for Research in Environmental
16 Science, University of Colorado Boulder, Boulder, CO, 80309, USA

17 [†]Now at Departments of Geology and Geophysics, and Applied Ocean Physics and Engineering, Woods Hole
18 Oceanographic Institution, Woods Hole, MA, 02543, USA

19 Correspondence to: Melisa A. Diaz (diaz.237@osu.edu/mdiaz@whoi.edu)

Field Code Changed

20 **Abstract.** ~~Modeling studies and field mapping show that increases in ice thickness during glacial periods were not~~
21 ~~uniform across Antarctica. Rather,~~ outlet glaciers that flow through the Transantarctic Mountains (TAM)
22 experienced ~~some of the greatest~~ changes in ice thickness ~~compared greater than to other coastal regions of~~
23 ~~Antarctica during glacial maxima.~~ As a result, ice-free areas that are currently exposed may have been covered by
24 ice at various points during the Cenozoic, complicating ~~the our~~ understanding of ecological succession in TAM
25 soils. ~~Our knowledge of glacial extent on small spatial scales is limited for the TAM, and studies of soil exposure~~
26 ~~duration and disturbance, in particular, are scattered rare.~~ We collected ~~surface soil surface~~ samples, and ~~in some~~
27 ~~places,~~ depth profiles every 5 cm to refusal (up to 30 cm) from eleven ice-free areas along the Shackleton Glacier, a
28 major outlet glacier of the East Antarctic Ice Sheet, (EAIS). ~~We explored the relationship between meteoric ^{10}Be and~~
29 ~~NO_3^- in these soils as a tool for understanding landscape disturbance and wetting history, and possibly as exposure~~
30 ~~proxies. Concentrations of meteoric ^{10}Be spanned more than an order of magnitude across the region (2.9×10^8~~
31 ~~atoms g^{-1} to 73×10^8 atoms g^{-1}) and are among the highest measured in polar regions. The concentrations of NO_3^-~~
32 ~~were similarly variable and ranged from $\sim 1 \mu\text{g g}^{-1}$ to 15mg g^{-1} . In examining differences and similarities in the~~
33 ~~concentrations of ^{10}Be and NO_3^- with depth, we suggest that much of the southern portion of the Shackleton Glacier~~
34 ~~region has likely developed under a hyper-arid climate regime with minimal disturbance. Finally, we attempted to~~
35 ~~determine inferred exposure time using ^{10}Be and NO_3^- concentrations as. This analysis, which suggests that the~~
36 ~~soils we analyzed likely range from recent exposure (following the Last Glacial Maximum) to possibly $>6 \text{Ma}$.~~
37 ~~While a small sample size, Our work data suggests that further testing and interrogation of meteoric ^{10}Be and NO_3^-~~
38 ~~concentrations and relationships in soils can provide critical important information regarding present landscape~~
39 ~~development, soil evolution processes, and inferred exposure durations of surfaces in for the TAM.~~

Formatted: Font: 12 pt

Formatted: Normal, Line spacing: single

42 We measured meteoric ^{10}Be and NO_3^- concentrations to calculate measured (using ^{10}Be inventory), estimated (using
43 NO_3^-), and inferred (using surface ^{10}Be concentration) surface exposure ages, both with and without assuming
44 erosion. Exposure ages ranged from 58 ka to >6.5 Ma correcting for erosion and 57 ka to 1.9 Ma without erosion,
45 with the youngest ages near the glacier terminus and at relatively lower elevations. We correlated NO_3^-
46 concentrations with meteoric ^{10}Be concentrations to estimate exposure ages for all locations with NO_3^- depth profiles
47 but only surface ^{10}Be data. Our results indicated that NO_3^- concentrations can be used in conjunction with few
48 meteoric ^{10}Be data to rapidly and efficiently estimate relative surface exposure ages. In comparing NO_3^- and ^{10}Be
49 depth profile measurements, we find that much of the southern portion of the Shackleton Glacier region has likely
50 developed undisturbed under a hyper arid climate regime.
51

52 1. Introduction

53 One of the most intriguing questions in biogeography concerns the relationship between the evolution of
54 terrestrial organisms and landscape disturbance (e.g., glacial overriding, soil wetting), particularly in Antarctica.
55 Current data indicate that organism lineages have survived in some Antarctic soils for possibly millions of years,
56 despite multiple glaciations throughout the Pleistocene (Convey et al., 2008; Fraser et al., 2012; Stevens and Hogg,
57 2003). It is still unclear how and where these organisms found suitable glacial refugia given the high salt
58 concentrations in high-elevation soils (Lyons et al., 2016). The most biodiverse soils in the Ross Sea sector are at
59 low elevations near the coast, where the Ross Ice Shelf or sea ice meet the Transantarctic Mountains (TAM) (Collins
60 et al., 2020). These soils are also those which are most susceptible to glacial overriding during glacial maxima,
61 though the timing of retreat and glacial extent is still unknown on local scales (Golledge et al., 2012; Mackintosh et
62 al., 2011).

63 Outlet glaciers are among the most sensitive areas to glaciological change in Antarctica, and changes in
64 their extents over time are recorded in nearby sedimentary deposits (Golledge et al., 2013; Jones et al., 2015;
65 Scherer et al., 2016; Spector et al., 2017). ~~However, only scattered information exists on TAM soil processes, ages,~~
66 ~~and chronosequences, and the implications for terrestrial and ecosystem history~~ (Bockheim, 2002; Dickinson et al.,
67 2012; Graham et al., 2002, 1997; Lyons et al., 2016; Scarrow et al., 2014; Schiller et al., 2009). The Shackleton
68 Glacier, an outlet glacier of the East Antarctic Ice Sheet (EAIS), flows between several exposed peaks of the Central
69 Transantarctic Mountains (CTAM) and ice-free areas are present at both low and high elevations. We report
70 concentrations of meteoric ^{10}Be and nitrate (NO_3^-) in soils from eleven distinct ice-free areas and investigate their
71 distributions at depth to ~~better understand wetting history, explore~~ ^{10}Be and NO_3^- relationships, ~~and infer exposure~~
72 ~~duration~~. The sampling methodology was designed to capture a range of soils which have low salt concentrations
73 due to recent exposure from glacial retreat following the Last Glacial Maximum (LGM) and soils that were likely
74 exposed since at least the last glacial period. These data ~~are~~ include some of the only meteoric ^{10}Be and NO_3^-
75 concentration data from the CTAM (Claridge and Campbell, 1968b, 1977; Graham et al., 1997; Lyons et al., 2016),
76 among few surface exposure ages in the CTAM (Aekert and Kurz, 2004; Balter-Kennedy et al., 2020), are the only
77 constrained age estimates of soils from the Shackleton Glacier region inform knowledge of landscape disturbance
78 and wetting history, eamay potentially be used to infer soil exposure duration, and inform how the EAIS responds
79 to changes in climate, and are crucial helpfuluseful in understanding Antarctic terrestrial biogeography.

81 2. Background

82 2.1. Brief overview of Antarctic glacial and wetting history

83 Antarctica is believed to have maintained a persistent ice sheet since at least the Eocene epoch, and the East
84 and West Antarctic Ice Sheets (EAIS and WAIS, respectively) have waxed and waned since at least the Miocene
85 (Gasson et al., 2016; Gulick et al., 2017). Sediment core records collected from the Ross Sea and ice cores from the
86 Antarctic interior indicate that the EAIS and WAIS have undergone dozens of glacial and interglacial cycles
87 throughout the Cenozoic (Augustin et al., 2004; Talarico et al., 2012). The WAIS is a marine-terminating ice sheet
88 with a grounding line below sea level, which decreases the stability of the ice sheet and results in rapid ~~ice sheet~~
89 advance and retreat ~~during glacial periods~~ compared to the EAIS (Pollard and DeConto, 2009). The EAIS is

90 grounded above sea level and is generally more stable ~~than the WAIS~~. The EAIS and WAIS were at their most
91 recent greatest extent about 14 ka during the Last Glacial Maximum (LGM) (~22,000 yrs. ago) (Clark et al., 2009).
92 During the LGM, the EAIS expanded along its margins and some of the greatest increases in height occurred at
93 outlet glaciers, which flow through exposed peaks of the TAM and drain into the Ross and Weddell Seas (Anderson
94 et al., 2002; Golledge et al., 2012; Mackintosh et al., 2014). As a result, many of the currently exposed TAM soils
95 were overrun by ice during the LGM and some may have only recently been exposed.

96 Much of the Antarctic continent is a polar desert and geomorphological data from ice-free soils in the
97 McMurdo Dry Valleys indicate that some regions have likely been hyper-arid for as long as 15 Ma (Marchant et al.,
98 1996; Valletta et al., 2015). As such, atmospherically-derived constituents, including salts and metals, can
99 accumulate in exposed Antarctic soils at concentrations similar to those from the Atacama and Namib Deserts (Diaz
100 et al., 2020; Lyons et al., 2016; Reich and Bao, 2018). Using soil NO₃ nitrate concentrations from the Meyer Desert
101 in the Beardmore Glacier region and NO₃ nitrate fluxes calculated from a Dominion Range ice core, Lyons et al.
102 (2016) estimated that at least 750,000 years have passed since the Meyer Desert had wide-spread soil wetting. It is
103 likely that other high elevation and inland locations in the TAM also have high concentrations of salts and similarly
104 old “wetting ages”, though this has not been thoroughly investigated.

105 Outlet glaciers are among the most sensitive areas to glaciological change in Antarctica, and changes in
106 their extents over time are recorded in nearby sedimentary deposits (Golledge et al., 2013; Jones et al., 2015;
107 Seherer et al., 2016; Spector et al., 2017). The Shackleton Glacier flows between several exposed peaks of the
108 Central Transantarctic Mountains (CTAM) and ice-free areas are present at both low and high elevations. We
109 calculated relative surface soil exposure ages of ice-free areas along the Shackleton Glacier, a major outlet glacier of
110 the EAIS. Outlet glaciers are among the most sensitive areas to glaciological change in Antarctica, and changes in
111 their extents over time are recorded in nearby sedimentary deposits (Golledge et al., 2013; Jones et al., 2015;
112 Seherer et al., 2016; Spector et al., 2017). The Shackleton Glacier flows between several exposed peaks of the
113 Central Transantarctic Mountains (CTAM) and ice-free areas are present at both low and high elevations. We report
114 concentrations of meteoric ¹⁰Be and nitrate (NO₃⁻) in soils from eleven distinct ice-free areas and use these data to
115 estimate the exposure ages using different assumptions. The sampling methodology was designed to capture soils
116 which have low salt concentrations due to recent exposure from glacial retreat following the LGM and soils that
117 were exposed since at least the last glacial period. These age data are among few surface exposure ages in the
118 CTAM (Ackert and Kurz, 2004; Balter-Kennedy et al., 2020), are the only age estimates of soils from the
119 Shackleton Glacier region, inform how the EAIS responds to changes in climate, and are crucial in understanding
120 Antarctic terrestrial biogeography.

121 **2. Background**

122 **2.2.1. Cosmogenic nuclide exposure age dating and meteoric ¹⁰Be systematics in Antarctic soils**

123 ¹⁰Be is a cosmogenic radionuclide with a half-life of 1.39 Ma (Korschinek et al., 2010) that is produced
124 both in the atmosphere (meteoric) and *in-situ* in mineral grains. In the atmosphere, N and O gases are bombarded by
125 high energy cosmic radiation to produce meteoric ¹⁰Be. Particle reactive ¹⁰BeO or ¹⁰Be(OH)₂ is produced and
126 removed from the atmosphere by wet and dry deposition (McHargue and Damon, 1991). At Earth's surface,
127 meteoric ¹⁰Be sorbs onto clay particles and ~~it~~ is insoluble in most natural waters of pH greater than 4 (Brown et al.,
128 1992; You et al., 1989). The clay particles can be redistributed to lower depths in the soils profile due to particle
129 migration or can be transported by winds. As such, the total number of ¹⁰Be atoms in a soil profile, its inventory, is a
130 function of surface exposure duration, erosion, clay particle translocation, solubility, and sedimentation. If delivery
131 rates can be ~~estimated~~determined, meteoric ¹⁰Be can be used as a tool to understand exposure ages, erosion rates,
132 and soil residence times (see Willenbring and Von Blanckenburg, 2009 and references within). There are scattered
133 exposure age studies from across the CTAM using a variety of *in-situ* produced cosmogenic nuclides (Ackert and
134 Kurz, 2004; Balter-Kennedy et al., 2020; Bromley et al., 2010; Kaplan et al., 2017; Spector et al., 2017), and

Formatted: Font: Italic

135 ~~previously reported exposure ages of CTAM moraines and boulders from these studies ranged from <10 ka to >14~~
136 ~~Ma.~~

137 The measurement of meteoric ^{10}Be in soil has enabled researchers to date surfaces (soils) and features in
138 Antarctica. Previous studies have measured meteoric ^{10}Be in the McMurdo Dry Valleys (MDV) and Victoria Land
139 soils and sediments to calculate exposure ages and to determine the onset of the current polar desert regime
140 (Dickinson et al., 2012; Graham et al., 2002; Schiller et al., 2009; Valletta et al., 2015). In general, these previous
141 studies found that high elevation, northern fringe regions along the Ross Embayment have been ice-free and
142 possibly hyper-arid since at least the Pliocene. Few meteoric ^{10}Be data have yet to be published from
143 the CTAM (Graham et al., 1997), which represent ice sheet dynamics and climatic conditions closer to the Polar
144 Plateau.

145 2.3.2. Nitrate systematics in Antarctic soils

146 The nitrogen cycle in Antarctica differs greatly from the nitrogen cycle in temperate regions, primarily due
147 to scarce biomass and few vascular plants (Cary et al., 2010; Michalski et al., 2005). Nitrogen in CTAM soils
148 primarily exists as nitrate (NO_3^-) and is primarily sourced from the atmosphere, with varying contributions from the
149 troposphere and stratosphere (Diaz et al., 2020; Lyons et al., 2016; Michalski et al., 2005). Similar to meteoric ^{10}Be ,
150 NO_3^- is deposited on exposed soils, though in contrast to ^{10}Be however, nitrate salts are highly water-soluble. Once
151 deposited on the surface, nitrate salts can be dissolved and transported to lower elevations down gradient or eluted
152 to depth when wetted (i.e., during ice/snow melt events). However, the hyper-arid climate of the CTAM can
153 allow NO_3^- to accumulate at high concentrations in soils (Claridge and Campbell, 1968a; Diaz et al., 2020; Lyons et
154 al., 2016). Soil NO_3^- concentrations have the potential to inform our knowledge of wetting history and possibly
155 glacial history in the CTAM due to the relatively high solubility of nitrate salts, though uncertainties regarding
156 heterogeneous deposition and post-depositional alteration (such as re-volatilization and photolysis) require further
157 investigation (Diaz et al., 2020; Frey et al., 2009; Graham et al., 2002).

158 2.3. Relative exposure age dating approach

159
160 Here, we used meteoric ^{10}Be and NO_3^- concentrations to estimate CTAM relative exposure ages,
161 acknowledging the widespread use of *in situ* exposure age dating which we later use for cross-validation. *In situ*
162 cosmogenic nuclides, such as ^{10}Be , ^{26}Al , ^{21}Ne , and ^3He , have been measured to determine surface exposure ages at
163 several locations across Antarctica, particularly in the MDV and other exposed surfaces in Victoria Land (e.g. Balco
164 et al., 2019; Brook et al., 1993, 1995; Bruno et al., 1997; Ivy-Ochs et al., 1995; Strasky et al., 2009). There are
165 considerably fewer studies from the CTAM (Ackert and Kurz, 2004; Balter-Kennedy et al., 2020; Bromley et al.,
166 2010; Kaplan et al., 2017; Spector et al., 2017), and previously reported exposure ages of CTAM moraines and
167 boulders from these studies ranged from <10 ka to >14 Ma. We seek to utilize NO_3^- and meteoric ^{10}Be
168 concentrations to attain a greater number of surface exposure ages and understand the relationship between NO_3^- and
169 ^{10}Be in the hyper-arid environment of the CTAM. Exposure ages are determined by three approaches: “measured”
170 by using measured meteoric ^{10}Be concentrations in depth profiles, “estimated” by using NO_3^- concentrations to
171 estimate ^{10}Be concentrations, and “inferred” by using the maximum/surface concentration of ^{10}Be in the soil profile
172 to infer the total number of ^{10}Be atoms in the profile (Graly et al., 2010). These approaches are described in Sections
173 4.3 and 5.3.

174 3. Study sites and region

175 Shackleton Glacier (~84.5 to 86.4°S; ~130 km long and ~10 km wide) is a major outlet glacier of the EAIS
176 that drains north into the Ross Embayment with other CTAM outlet glaciers to form the Ross Ice Shelf (RIS) (Fig.
177 1). The ice flows between exposed surfaces of the Queen Maud Mountains, which range from elevations of ~150 m
178 near the RIS to >3,500 m further inland. The basement geology of the Shackleton Glacier region is comprised of
179 igneous and metamorphic rocks that formed from intruded and metamorphosed sedimentary and volcanic strata

180 during the Ross Orogeny (450-520 Ma) (Elliot and Fanning, 2008). The southern portion of the region consists of
181 the Devonian-Triassic Beacon Supergroup and the Jurassic Ferrar Group, while the northern portions consists of
182 Pre-Devonian granitoids and the Early to Mid-Cambrian Taylor Group (Elliot and Fanning, 2008; Paulsen et al.,
183 2004). These rocks serve as primary parent material for soil formation (Claridge and Campbell, 1968b). Deposits of
184 the Sirius Group, the center of the stable vs. dynamic EAIS debate, have been previously identified in the southern
185 portion of the Shackleton Glacier region, particularly at Roberts Massif (Fig. 2) and Bennett Platform, with a small
186 exposure at Schroeder Hill (Hambrey et al., 2003).

187 The valleys and other ice-free areas within the region have been modified by the advance and retreat of the
188 Shackleton Glacier, smaller tributary glaciers, and alpine glaciers. Similar to the Beardmore Glacier region, the
189 Shackleton Glacier region is a polar desert, which results in the high accumulation of salts in soils. The surface is
190 comprised primarily of till, weathered primary bedrock, and scree, which ranges in size from small boulders and
191 cobbles to sand and silt. Clay minerals have been previously identified in all samples from Roberts Massif and are
192 likely ubiquitous throughout the region (Claridge and Campbell, 1968b). ~~However, the~~The clays are a mixture of
193 those derived from sedimentary rocks and contemporaneous weathering (Claridge and Campbell, 1968b). Thin,
194 boulder belt moraines, characteristic of cold-based glaciers, were deposited over bedrock and tills at Roberts Massif,
195 while large moraines were deposited at Bennett Platform (Fig. 2; Balter-Kennedy et al., 2020; Claridge and
196 Campbell, 1968). Most soils appeared dry, though some small ponds and water tracks have been documented near
197 Mt. Heekin and Thanksgiving Valley (Elliot et al., 1996). Additional information on the sample locations and
198 surface features is provided in Tables 1 and 2.

199 4. Methods

200 4.1. Sample collection

201 During the 2017-2018 austral summer, we visited eleven ice-free areas along the Shackleton Glacier:
202 Roberts Massif, Schroeder Hill, Bennett Platform, Mt. Augustana, Mt. Heekin, Thanksgiving Valley, Taylor
203 Nunatak, Mt. Franke, Mt. Wasko, Nilsen Peak, and Mt. Speed (Fig. 1). These areas represent soils from near the
204 head of the glacier to near the glacier terminus at the coast of the RIS. Two surface samples (Table 1) were collected
205 at each location (except for Nilsen Peak and Mt. Wasko, represented by only one sample each) with a plastic scoop
206 and stored in Whirl-Pak™ bags. One sample was collected furthest from the Shackleton Glacier or other tributary
207 glaciers (within ~2,000 m) to represent soils that were likely exposed during the LGM and previous recent glacial
208 periods. A second sample was collected closer to the glacier (between ~1,500 and 200 m from the first sample) to
209 represent soils likely to have been covered during the LGM and exposed by more recent ice margin retreat.

210 Soil pits were dug by hand at the sampling locations furthest from the glacier for Roberts Massif, Schroeder
211 Hill, Mt. Augustana, Bennett Platform, Mt. Heekin, Thanksgiving Valley, and Mt. Franke (7 sites). Continuous
212 samples were collected every 5 cm until refusal (up to 30 cm) and stored frozen in Whirl-Pak™ bags. All surface
213 (21) and depth profile (25) samples were shipped frozen to The Ohio State University and kept frozen until
214 analyzed. We selected Roberts Massif, Bennett Platform, and Thanksgiving Valley as locations for the most in-
215 depth analysis for the depth profiles. These locations were chosen to maximize variability in landscape
216 development: Roberts Massif represented an older, likely minimally disturbed landscape; Thanksgiving Valley
217 represented a landscape with possible hydrologic activity, as evidenced by nearby ponds; Bennett Platform
218 represented a landscape with evidence of recent glacial advance and retreat, and substantial topographic highs and
219 lows (Table 2).

220 4.2. Analytical methods

221 4.2.1. Meteoric ¹⁰Be analysis

222 A total of 30 sub-samples of surface soils from all locations, and the depth profiles from Roberts Massif,
223 Bennett Platform, and Thanksgiving Valley, were sieved to determine the grain size at each location. For each
224 sample, the percentages of gravel (>2 mm), sand (63 μm-2 mm), and silt (<63 μm) are reported in Table S1. Since
225 there is a strong grain size dependence of meteoric ¹⁰Be (little ¹⁰Be is carried on coarse (>2 mm) grains (Pavich et

226 al., 1986)) the gravel portion of the sample was not included in the meteoric ^{10}Be analysis. The remaining soil (<2
227 mm) was ground to fine powder using a shatterbox.

228 Meteoric ^{10}Be (Table-Table 1; S22) was extracted and purified at the NSF/~~UVM~~ University of Vermont
229 (UVM) Community Cosmogenic Facility following procedures originally adapted and modified from Stone (1998).
230 First, 0.5 g of powdered soil was weighed into platinum crucibles and 0.4 g of SPEX ^9Be carrier (with a
231 concentration of $1,000 \mu\text{g mL}^{-1}$) was added to each sample. The samples were fluxed with a mixture of potassium
232 hydrogen fluoride and sodium sulfate. Perchloric acid was then added to remove potassium by precipitation and later
233 evaporated. Samples were dissolved in nitric acid and precipitated as beryllium hydroxide ($\text{Be}(\text{OH})_2$) gel, then
234 packed into stainless steel cathodes for accelerator mass spectroscopy-spectrometer isotopic analysis at the Purdue
235 Rare Isotope Measurement (PRIME) Laboratory. Isotopic ratios were normalized to primary standard 07KNSTD
236 with an assumed ratio of 2.85×10^{-12} (Nishiizumi et al., 2007). We corrected sample ratios with a $^{10}\text{Be}/^9\text{Be}$ blank
237 ratio of $8.2 \pm 1.9 \times 10^{-15}$, which is the average and standard deviation of two blanks processed alongside the samples.
238 We subtracted the blank ratio from the sample ratios and propagated uncertainties in quadrature. Blank correction is
239 not significant.

240 4.2.2. Nitrate- NO_3^- analysis

241 Separate, un-sieved sub-samples of soil from all locations and depth profiles were leached at a 1:5 soil to
242 DI water ratio for 24 hours, then filtered through a $0.4 \mu\text{m}$ Nucleopore membrane filter. The leachate was analyzed
243 on a Skalar San++ Automated Wet Chemistry Analyzer with an SA 1050 Random Access Auto-sampler (Lyons et
244 al., 2016; Welch et al., 2010). Concentrations are reported as NO_3^- (Table S21) with accuracy, as determined using a
245 USGS 2015 "round-robin" standard, and precision better than 5% (Lyons et al., 2016).

246 4.3. Exposure age model/Meteoritic ^{10}Be inventory

247 We developed a mass balance using the fluxes of meteoric ^{10}Be to and from Shackleton Glacier region soils
248 to calculate the amount of time which has passed since the soil was exposed/understand the accumulation of ^{10}Be in
249 glaciated environments (Pavich et al., 1984, 1986). The model assumes that soils that were overlain by glacial ice in
250 the past and are now exposed, accumulated less ^{10}Be than soils that were exposed throughout the glacial periods
251 (Fig. 3). The concentration of meteoric ^{10}Be at the surface (N , atoms g^{-1}) per unit of time (dt) is expressed as a
252 function, where the addition of ^{10}Be is represented as the atmospheric flux to the surface (Q , atoms $\text{cm}^{-2} \text{yr}^{-1}$), and
253 removal is due to both radioactive decay, which is represented by a disintegration constant (λ , yr^{-1}), and erosion
254 (E , cm yr^{-1}) is with respect to soil density (ρ , g cm^{-3}) (Eq. 1). Particle mobility into the soil column is represented by
255 a diffusion constant (D , $\text{cm}^2 \text{yr}^{-1}$) multiplied by a concentration gradient. The differential in depth is represented by
256 dz .

$$257 \frac{dN}{dt} = Q - \lambda N - E \frac{dN}{dz} - D \frac{d^2N}{dz^2} \quad (1)$$

258 However, this function is highly dependent on dz , which represents an unknown value of depth into the soil
259 column which is influenced by meteoric ^{10}Be deposition and removal. Additionally, the soil diffusion term is
260 unconstrained and likely varies with depth. We accounted for these uncertainties and other uncertainties regarding
261 ^{10}Be migration in the soil column by calculating the inventory (I , atoms cm^{-2}) of the soil (Eq. 2) (Pavich et al.,
262 1986). We used a density (ρ) of 2 g cm^{-3} , assuming and assumed that Q had not changed systematically over the
263 accumulation interval (Craly et al., 2010; Pavich et al., 1986). The inventory is the total sum of meteoric ^{10}Be atoms
264 in the soil profile and the change in inventory due to deposition, decay, and surface erosion is related surface
265 exposure age-duration (Eq. 3).

$$266 I = \sum N \cdot \rho \cdot dz \quad (2)$$

$$267 \frac{dI}{dt} = Q - \lambda I - EN \quad (3)$$

268 If the inventory of meteoric ^{10}Be in the soil profile, the concentration at the surface, and soil density are
269 known, and published values for erosion and ^{10}Be flux to the surface are used, we can combine Eqs. (1-3), and solve
270 for time (t , years) (Eq. 4):

$$271 \quad t = -\frac{z}{\lambda} \cdot \ln \left[1 - \frac{\lambda I}{Q - E \rho N} \right] \quad (4)$$

272 Equation (4) provides a maximum exposure age assuming that the soil profile did not contain meteoric ^{10}Be
273 before it was exposed to the surface ($N_0 = 0$). Since our exposure age dating technique relies on the number of ^{10}Be
274 atoms within the sediment column (I), any pre-existing ^{10}Be atoms in the soil ($N_0 \neq 0$) causes the calculated age to
275 be an overestimate (Fig. 3c-d) (Graly et al., 2010). Meteoric ^{10}Be concentrations typically decrease with depth until
276 they reach a “background” level (Graly et al., 2010). The background is identified as the point where the
277 concentration of meteoric ^{10}Be is constant with depth ($\frac{dN}{dz} = 0$). Typically, the background values can be used to
278 calculate an initial inventory (I_i , atoms cm^{-2}) using Eq. (45), where N_z is the ^{10}Be concentration (atoms g^{-1}) at the
279 bottom of the profile (z , cm), and correct the observed total inventory (Eq. 6). In this case, we assume that the initial
280 concentration of meteoric ^{10}Be is isotropic. However, an accurate initial inventory can only be determined for soil
281 profiles that are deep enough to capture background concentrations which decrease in ^{10}Be concentrations to
282 background levels due to the downward transport of ^{10}Be from the surface. This may not be the case in areas of
283 permafrost where ^{10}Be is restricted to the active layer (Bierman et al., 2014).

$$284 \quad I_i = N_z \cdot \rho \cdot z \quad (45)$$

$$285 \quad t = -\frac{z}{\lambda} \cdot \ln \left[1 - \frac{(I - I_i)\lambda}{Q - E \rho N} \right] \quad (6)$$

286 Additionally, the initial inventory can be influenced by repeated glacial advance and retreat during
287 glacial-interglacial cycles. For this case, the soil has “inherited” ^{10}Be during each subsequent exposure to the
288 atmosphere, some of which may have been removed with eroded soil (Fig. 3c-d). For constructional landforms, such
289 as moraines, the inheritance is equal to the background/initial inventory. Without information on drift sequences, it
290 is difficult to correct the measured inventory for inheritance by distinguishing meteoric ^{10}Be that was deposited after
291 the most recent ice retreat from ^{10}Be that was deposited during previous interglacial periods. Instead, only ages that
292 represent total time of exposure through glacial-interglacial cycles, likely as overestimates, can be reported with
293 confidence.

294 4.3.1. Model variable selection and key assumptions

295 The exposure age calculations are dependent on the selected values for the variables in Eq. (1-6). We chose
296 a flux value (Q) of 1.3×10^5 atoms $\text{cm}^{-2} \cdot \text{yr}^{-1}$ from Taylor Dome (Steig et al., 1995) due to a similar climate to that of
297 the CTAM and an absence of local meteoric ^{10}Be flux data. Soil density (ρ) across the Shackleton Glacier region
298 was approximately 2 g cm^{-3} . While we did not calculate erosion rates, previous studies have estimated rates from
299 rocks of 1 to 65 cm Ma^{-1} in Victoria Land (Ivy-Ochs et al., 1995; Margerison et al., 2005; Morgan et al., 2010;
300 Strasley et al., 2009; Summerfield et al., 1999) and 5 to 35 cm Ma^{-1} further south in the Transantarctic Mountains
301 (Aekert and Kurz, 2004; Balter-Kennedy et al., 2020; Morgan et al., 2010). Balter-Kennedy et al. (2020) determined
302 that erosion rates for boulders at Roberts Massif which were less than 2 cm Ma^{-1} . However, we chose a conservative
303 value of 5 cm Ma^{-1} for our analysis of the Shackleton Glacier region.

304 It is important to note two key assumptions in our variable selection and model development. First, we have
305 assumed a uniform erosion rate across the region. Given the variety of surface features at each location (Table 2),
306 some locations on valley floors, for example, may have increased surface concentrations of meteoric ^{10}Be due to
307 entrapment of wind-blown fine-grained sediments. Locations on hillslopes and valley walls might have higher
308 erosion rates (Morgan et al., 2010; Schiller et al., 2009). We assumed that deflation of fine-grained material had
309 occurred rapidly on the flat surfaces we sampled due to strong winds over the poorly consolidated tills following soil
310 exposure (Lancaster et al., 2010). Due to a deficit of soil erosion data in the CTAM, we calculated exposure ages

Field Code Changed

(Eq. 6) with the 5 cm Ma⁻¹ erosion value and without the erosion/deposition term ($E=0$). Second, we attempted to estimate the background concentrations and initial inventory for each sample collected furthest from the glacier. We hypothesized that these samples were potentially exposed throughout at least the LGM and had negligible inheritance, though this was merely an assumption. With the possibility of overestimating or underestimating the exposure ages, we solved Eq. 6 both with and without estimated initial inventory terms. For all samples, including those without depth profile measurements, we utilized an empirical relationship derived between surface/maximum meteoric ¹⁰Be concentration and measured inventory to estimate surface exposure ages (see Section 5.3.3) (Graly et al., 2010). Regarding our NO₃⁻ measurements, we assumed that aside from solubilization and salt translocation, NO₃⁻ is preserved in the soils and any volatilization or photolysis is negligible (Diaz et al., 2020; Jackson et al., 2016).

5. Results

5.1. Depth profile composition Concentrations and concentrations of meteoric ¹⁰Be and depth profile composition

Sediment grain size is similar among the three soil profiles collected from Roberts Massif, Bennett Platform, and Thanksgiving Valley; the soils are primarily comprised of sand-sized particles, with less silt-sized and smaller material (Fig. 4). The proportions of silt and gravel are similar at Roberts Massif, although the majority of the profile is sand-sized. Thanksgiving Valley has the coarsest-least fine material, while Bennett Platform has a more even grain size distribution. The deepest profile is from Thanksgiving Valley, while the Roberts Massif and Bennett Platform profiles are half the depth. All three profiles are ice-cemented at the bottom and are shallow compared to those collected from the McMurdo Dry Valleys (Dickinson et al., 2012; Schiller et al., 2009; Valletta et al., 2015), though they are comparable to profiles collected at Roberts Massif by Graham et al. (1997).

Surface concentrations of meteoric ¹⁰Be for both surface and depth profiles samples span more than an order of magnitude in the Shackleton Glacier region and range from 2.9 x 10⁸ atoms g⁻¹ at Mount Speed to 73 x 10⁸ atoms g⁻¹ at Roberts Massif (Fig. 5; Table 1). At individual sites where samples were collected at two locations, concentrations are typically highest for the samples furthest from the glacier, with notable exceptions at Roberts Massif and Thanksgiving Valley (Fig. 5). This trend is expected since our sampling plan was designed to capture both recently exposed soils (near the glacier(s)) and soils which have been exposed throughout the LGM and possibly other glacial periods. The measured inventories (Eq. 2) vary from 0.57 x 10¹¹ atoms at Bennett Platform to 1.5 x 10¹¹ atoms at Roberts Massif (Table 3).

The meteoric ¹⁰Be depth profiles differ between Roberts Massif, Bennett Platform, and Thanksgiving Valley, and Bennett Platform. The profile from Roberts Massif has the highest overall concentrations (Fig. 6). Within the profile, the 5-10 cm sampling interval has the highest concentration, followed by the bottom of the profile, then the surface. The profile behavior for Thanksgiving Valley is similar, though the differences in concentrations within both profiles are relatively small. Bennett Platform is the only location where the surface concentration is the highest compared to the remainder of the profile. Concentration, which and the concentration decreases with depth (Fig. 6). Although we sampled the entirety of the active layer where modern particle mobility throughout the soil column occurs, no depth profiles appear to decrease to background levels needed to calculate an initial meteoric ¹⁰Be inventory (Eq. 54). As a result, we are not able to correct the measured inventory for background ¹⁰Be, nor are we able to estimate the inherited ¹⁰Be concentration in the soil (Eq. 6).

5.2. Relationship between meteoric ¹⁰Be and Variability of NO₃⁻:NO₃⁻

Measured concentrations of NO₃⁻ span four orders of magnitude across the seven depth profiles we sampled in the Shackleton Glacier region (Fig. S16; Table S21). The lowest concentration is from Mt. Franke, at ~1 μg g⁻¹; the highest concentration is from Roberts Massif, at 15 mg g⁻¹. In addition, similar to the meteoric ¹⁰Be profiles, the NO₃⁻ concentrations are highest for the samples that were collected furthest from the coast and at the highest elevations (Table S2). The concentrations of NO₃⁻ and meteoric ¹⁰Be are compared for Roberts Massif, Bennett Platform, and Thanksgiving Valley (Fig. 6b). In general, the profiles from Roberts Massif and Thanksgiving Valley are similar (Fig. 6b); where ¹⁰Be and NO₃⁻ concentrations are highest just below the surface in the 5-10 cm interval

357 and are fairly consistent throughout the profile. The NO_3^- depth profile mirrors the ^{10}Be profile at Bennett Platform –
358 while ^{10}Be concentrations decrease with depth, the NO_3^- concentration increases with depth.

359 Since we measured NO_3^- concentrations for all seven depth profiles we collected, we compare the profile
360 concentrations and shapes from the four profiles without ^{10}Be depth measurements (Mt. Augustana, Schroeder Hill,
361 Mt. Franke, and Mt. Heekin) to the Roberts Massif, Bennett Platform, and Thanksgiving Valley profiles with both
362 measurements (Fig. 6). Most of the NO_3^- profiles do not significantly change with depth and are similar to the
363 profile from Thanksgiving Valley, though Schroeder Hill is most similar to Roberts Massif (Fig. 6). This is
364 unsurprising given the similar latitudes, surface features, and environmental conditions between the different
365 locations (e.g., high latitude hyper-arid vs. lower latitude with possible evidence of wetter conditions) (Fig. 1; Table
366 2). No other location had large terminal moraines, as observed at Bennett Platform.

367 Since the behaviors of NO_3^- and ^{10}Be are parallel or mirrored (as in the case for Bennett Platform), we
368 further evaluate their relationship. When regressed on log scales, NO_3^- and ^{10}Be have a strong power-law
369 relationship with R^2 values ranging from 0.66 to 0.99 (Fig. 6c). The power-law slope for Roberts Massif and
370 Thanksgiving Valley is positive, while the Bennett Platform has a negative slope. Given this regressed relationship,
371 it is possible to estimate ^{10}Be concentrations using NO_3^- concentrations (see Section 5.3.2).

372 **5.3. Relative exposure age calculations and estimates**

373 **5.3.1 “Measured” exposure ages from Roberts Massif, Bennett Platform, and Thanksgiving Valley**

374 We calculated exposure ages for the samples furthest from the glacier for Roberts Massif, Bennett
375 Platform, and Thanksgiving Valley using Eq. 4, both with and without the erosion term (Table 3). The exposure
376 ages with erosion range from 120 ka to 4.15 Ma, and the ages without erosion range from 110 ka to 1.67 Ma for
377 Bennett Platform and Roberts Massif, respectively. Thanksgiving Valley is intermediate with an exposure age of
378 540 ka with erosion and 500 ka without erosion. Since we are not able to correct for initial inventory or inheritance,
379 the exposure ages with the erosion term represent maximum ages. The erosion rate we estimated is relatively low
380 compared to the calculated exposure ages for most samples and would only slightly influence the measured
381 exposure ages. Roberts Massif is an exception where the inclusion or exclusion of erosion alters the measured age
382 by over 50%. Moreover, the ages without erosion terms are probably overestimates as well without inheritance
383 corrections.

384 **5.3.2 “Estimated” exposure ages using NO_3^- relationship**

385 Since the behaviors of NO_3^- and ^{10}Be are parallel or mirrored (as in the case for Bennett Platform), we
386 further evaluate their relationship. When regressed on log scales, NO_3^- and ^{10}Be have a strong power-law
387 relationship with R^2 values ranging from 0.66 to 0.99 (Fig. 6c). The power-law slope for Roberts Massif and
388 Thanksgiving Valley is positive, while the Bennett Platform has a negative slope. Given this regressed relationship,
389 it is possible to estimate ^{10}Be concentrations using NO_3^- concentrations (see Section 5.3.2).

390 As we suggest in Section 5.2, the power-law relationship between NO_3^- and meteoric ^{10}Be can be used to
391 estimate ^{10}Be concentrations from NO_3^- concentrations. Since we measured NO_3^- concentrations in all seven depth
392 profiles, we compared the profile concentrations and shape from the four profiles without ^{10}Be depth measurements
393 (Mt. Augustana, Schroeder Hill, Mt. Franke, and Mt. Heekin) to the Roberts Massif, Bennett Platform, and
394 Thanksgiving Valley profiles with both measurements (Fig. S1). Our calculation fundamentally assumes no loss of
395 NO_3^- due to prolonged surface exposure and that NO_3^- profiles which have similar shapes among the sites might
396 have similar ^{10}Be profile shapes as well. The profiles are all fairly homogenous and most similar to the profile from
397 Thanksgiving Valley, though Schroeder Hill is most similar to Roberts Massif (Fig. S1). Applying the power-law
398 relationship from Thanksgiving Valley to Mt. Augustana, Mt. Franke and Mt. Heekin, and the relationship from
399 Roberts Massif to Schroeder Hill, we provide estimates of meteoric ^{10}Be concentrations for the entire depth profile
400 (Table S2) and use these concentrations to calculate an “estimated” inventory using Eq. 2 (Table 4). Further, the
401 estimated inventories are used to estimate exposure ages using Eq. 4, both with and without the erosion term.

402 The estimated inventories (using the NO_3^- -power law relationship) with erosion range from 0.14×10^{14}
403 atoms at Bennett Platform to 1.5×10^{14} atoms at Roberts Massif (Table 4). The measured and estimated inventories
404 differ by $\sim 3-18\%$. The estimated exposure ages using the estimated inventory range from 120 ka to 4.54 Ma with
405 erosion, and the ages without erosion range from 110 ka to 1.74 Ma for Bennett Platform and Roberts Massif,
406 respectively (Table 4). The measured and NO_3^- -estimated exposure ages, both with and without erosion, only differ
407 by $\sim 4-20\%$ for Roberts Massif, Bennett Platform, and Thanksgiving Valley. Since we cannot calculate exposure
408 ages using only ^{10}Be for the profiles from Schroeder Hill, Mt. Augustana, Mt. Heekin, and Mt. Franke, we are not
409 able to make similar age comparisons. However, we can compare the estimated surface ^{10}Be concentrations using
410 NO_3^- to the measured ^{10}Be concentrations. The percent differences at Schroeder Hill and Mt. Heekin are 4% and 7%,
411 respectively, while Mt. Augustana and Mt. Franke have higher differences of 36% and 40%, respectively (Tables 3
412 and S2).

413 5.3.3 “Inferred” exposure ages using inventory relationship

414 Similar to our exposure age estimates using NO_3^- concentrations, we used the relationship between the
415 maximum meteoric ^{10}Be concentration in the soil profile and the meteoric ^{10}Be inventory (Graly et al., 2010) to
416 “infer” ^{10}Be inventories and calculate maximum exposure ages for all eleven locations, again, with and without
417 erosion (Fig. 7; Table 5). As is the case for Roberts Massif and Thanksgiving Valley, the highest concentrations may
418 not always be at the surface for all locations; however, the relationship is sufficiently strong to provide an estimate
419 of the ^{10}Be inventory and thus an age estimate (Fig. 7). Compared to the measured inventories from Roberts Massif,
420 Bennett Platform, and Thanksgiving Valley, the inferred inventories differ by $\sim 16-130\%$. The inferred exposure
421 ages with erosion range from 58 ka to >6.5 Ma, and the ages without erosion range from 57 ka to 1.94 Ma for Mt.
422 Speed and Roberts Massif, respectively (Table 4). With the exception of Roberts Massif, Thanksgiving Valley, and
423 Mt. Speed, the oldest surfaces are those which we sampled furthest from the glacier, which is consistent with our
424 sampling methodology to capture younger and older soils. The sample from Roberts Massif collected closest to the
425 glacier has an estimated exposure age that is outside the model limits (>6.5 Ma). The measured exposure ages and
426 the inferred exposure ages differ by $\sim 49-75\%$ with erosion and $\sim 15-75\%$ without erosion. The greatest differences
427 between the ages are at Bennett Platform.

428 6. Discussion

429 Meteoric ^{10}Be concentrations and surface exposure ages vary widely across the Shackleton Glacier region
430 and at individual locations. Although these data are only measurements from discrete points on the landscape, they
431 constrain relative terrestrial exposure ages. These meteoric ^{10}Be and NO_3^- data contribute to growing exposure age
432 measurements, which can inform climate, landscape development, and biogeography. The Shackleton Glacier region
433 soil profiles and surface samples have are have are among the highest meteoric ^{10}Be concentrations ($\sim 10^9$ atoms g^{-1})
434 yet measured in Earth’s polar regions (Fig. 6a). Though our profiles are shallower than profiles from the MDV and
435 Victoria Land in Antarctica (Dickinson et al., 2012; Schiller et al., 2009; Valletta et al., 2015) and Sweden and
436 Alaska in the Arctic (Bierman et al., 2014; Ebert et al., 2012), the soils from these previous studies reached
437 background concentrations of ^{10}Be within the top 40 cm, which is close to our maximum depth of 30 cm at
438 Thanksgiving Valley. For comparison, the deepest profile collected by Graham et al. (1997) at Roberts Massif was
439 36 cm. The Bennett Platform soil profile is most similar to the soil profiles from other regions in Antarctica, as they
440 have decreasing ^{10}Be concentrations with depth, while Thanksgiving Valley and Roberts Massif are relatively
441 homogenous and more similar to profiles from the Arctic.

442 The inventories from this study are also among the highest calculated for Antarctic soils. The inventories
443 from Bennett Platform and Thanksgiving Valley are most similar ($\sim 10^{10}$) to inventories of saprolites and tills from
444 Sweden (Ebert et al., 2012) and the MDV (Schiller et al., 2009), though higher than those measured from other high
445 elevation, inland locations in Victoria Land (Dickinson et al., 2012; Valletta et al., 2015). Our inventory from
446 Roberts Massif is the same as the inventory reported for a nearby location by Graham et al. (1997), and all of our
447 inventories are within the range of values from the Arctic (Bierman et al., 2014), despite shallower profiles.

448 **6.1. Relationships between meteoric ¹⁰Be and NO₃⁻ and governing processes**

449 Previous studies have argued/proposed that atmosphere-derived salt concentrations at the surface may
450 correlate with exposure ages and wetting ages in Antarctica (Everett, 1971; Graham et al., 2002, 1997; Graly et al.,
451 2018; Lyons et al., 2016; Schiller et al., 2009). Graly et al. (2018) showed that, in particular, water-soluble NO₃⁻ and
452 boron exhibited the strongest relationships with exposure age (R² = 0.9 and 0.99, respectively). Lyons et al. (2016)
453 used NO₃⁻ concentrations to estimate the amount of time since the soils were last wetted, and Graham et al. (2002)
454 attempted to calculate exposure ages using the inventory of NO₃⁻ in the soil. Graly et al. (2018) argue that boron is
455 the best exposure proxy due to concerns related to NO₃⁻ mobility under sub-arid conditions (e.g. Frey et al., 2009;
456 Michalski et al., 2005), and given that uncertainties in local accumulation rates and ion transport can result in
457 inaccurate ages when using NO₃⁻ alone (Graham et al., 2002; Schiller et al., 2009). Based on the results presented
458 here for hyper-arid CTAM ice-free regions and the concerns with boron mobility depending on whether the B
459 species present in the soils is BO₃³⁻ (borate) or H₃BO₃ (boric acid), we suggest that NO₃⁻ is suitable for interpreting
460 wetting and disturbance histories.

461 Both meteoric ¹⁰Be and NO₃⁻ are sourced from atmospheric deposition in the Shackleton Glacier region,
462 and there appears to be a relationship between the two constituents in the soil profiles (Fig. 6b). A similar
463 relationship between soluble salts and meteoric ¹⁰Be was previously documented at Roberts Massif (Graham et al.,
464 1997). NO₃⁻ is highly mobile in wetter systems, while ¹⁰Be is less mobile under circumneutral pH. Given sustained
465 hyper-arid conditions, minimal landscape disturbance, and negligible biologic activity, one can expect meteoric ¹⁰Be
466 and NO₃⁻ to be correlated throughout a depth profile given the similar accumulation mechanism (Everett, 1971;
467 Graham et al., 1997). Further, their inventories (Eq. 2) should increase monotonically with exposure duration.
468 Deviations from this expected relationship would possibly could be due to 1) soil wetting, either in the present or
469 past, 2) deposition of sediment with different ¹⁰Be to NO₃⁻ ratios compared to the depositional environment, 3)
470 changes in the flux of either ¹⁰Be or NO₃⁻ with time, and 4) additional loss of NO₃⁻ due to denitrification or
471 volatilization. The latter two mechanisms are likely minor processes, however, NO₃⁻ deposition fluxes are known to
472 be spatially variable (Jackson et al., 2016; Lyons et al., 1990). As stated previously described above, Roberts Massif,
473 Bennett Platform, and Thanksgiving Valley were selected for further investigation as locations which may represent
474 different depositional environments: hypothesized hyper-aridity, recent glacial activity with large moraines, and
475 active hydrology, respectively. By comparing differences in the expected and observed relationship between ¹⁰Be
476 and NO₃⁻, we can possibly infer the processes which have influenced their relationship.

477 **6.1.2. NO₃⁻ as an Implications for landscape disturbance and paleoclimate**
478 **efficient inventory and exposure age estimation tool**

479 This is the first study to use NO₃⁻ concentrations to directly estimate meteoric ¹⁰Be concentrations study,
480 but not the first to attempt to use water-soluble NO₃⁻ and salts to help understand glacial history. Previous studies
481 have argued that atmosphere-derived salt concentrations at the surface may correlate with exposure ages and wetting
482 ages in Antarctica (Everett, 1971; Graham et al., 2002, 1997; Graly et al., 2018; Lyons et al., 2016; Schiller et al.,
483 2009). Graly et al. (2018) showed that, in particular, water-soluble NO₃⁻ and boron exhibited the strongest
484 relationships with exposure age (R² = 0.9 and 0.99, respectively). Lyons et al. (2016) used nitrate concentrations to
485 estimate the amount of time since the soils were last wetted and Graham et al. (2002) attempted to calculate
486 exposure ages using the inventory of nitrate in the soil. Graly et al. (2018) argue that boron is preferable to nitrate
487 due to concerns related to nitrate mobility under sub-arid conditions (e.g. Frey et al., 2009; Michalski et al., 2005),
488 and given that uncertainties in local accumulation rates and ion transport can result in inaccurate ages when using
489 NO₃⁻ alone (Graham et al., 2002; Schiller et al., 2009). Based on the results presented here for hyper-arid CTAM
490 ice-free regions and the concerns with boron mobility depending on whether the B species present in the soils is
491 BO₃³⁻ (borate) or H₃BO₃ (boric acid), we conclude that NO₃⁻ appears suitable for relative age dating and for
492 producing age estimates.

493 We show that the differences between measured ¹⁰Be inventories and estimated inventories using NO₃⁻ are
494 low (see Section 5.3.2) and argue that the power-law relationship between meteoric ¹⁰Be and NO₃⁻ can be used to

495 expand our current exposure age database for the TAM; compared to cosmogenic radionuclide analyses, NO₃⁻
496 analyses are rapid and cost effective. However, a model using NO₃⁻ or salts alone is likely insufficient, unless the
497 anion accumulation rates are known (Graham et al., 2002; Schiller et al., 2009). Though the regressions between
498 NO₃⁻ and ¹⁰Be are strong (Fig. 6c), each of the three profiles from Roberts Massif, Bennett Platform, and
499 Thanksgiving Valley have different regression coefficients and slopes. In other words, the nature of the relationship
500 between meteoric ¹⁰Be and NO₃⁻ varies across the Shackleton Glacier region and varies depending on the location.
501 This is likely due to differences in NO₃⁻ and ¹⁰Be transport and mobility in different surface environments and under
502 different local climates. To address these uncertainties, some ¹⁰Be data (surface samples for all locations and a few
503 depth profiles) are necessary to constrain the most accurate regression and minimize the associated error.

504 We tested our meteoric ¹⁰Be – NO₃⁻ model with data from Arena Valley in the MDV (Graham et al., 2002)
505 and found that our model is applicable to other TAM ice-free areas. Similar to the Shackleton Glacier region soils,
506 the soils from Arena Valley are hyper-arid with high concentrations of NO₃⁻ and other salts (Graham et al., 2002).
507 Precipitation in the MDV is low at ~5 cm water equivalent each year (Fountain et al., 1999), though NO₃⁻ and other
508 water-soluble salts at the surface can be wetted and mobilized. The highest NO₃⁻ concentrations are at 10 cm depth,
509 while ¹⁰Be concentrations are highest at the surface and decrease with depth, indicating vertical transport of NO₃⁻
510 through time (Graham et al., 2002). The power-law relationship between ¹⁰Be and NO₃⁻ throughout the profile is
511 weaker for the Arena Valley samples compared to Shackleton Glacier samples; there is a stronger power-law
512 correlation in the top 20 cm (R² = 0.61) compared to the bottom 70 cm (R² < 0.01), though the profile is
513 considerably deeper (110 cm). Using the power-law relationship from Bennett Platform, which mostly closely
514 resembles the profile behavior for Arena Valley given the negative regression slope, the estimated inventory is 5.4 x
515 10¹⁰ atoms. The measured inventory is of the same order of magnitude, 1.3 x 10¹⁰ atoms, indicating a moderate
516 model fit. Applying the power-law relationship from Arena Valley, the estimated inventory is 9.2 x 10⁹ atoms,
517 which is ~27% lower than the measured inventory. These results indicate that, although the Shackleton Glacier
518 region is nearly 900 km from Arena Valley, the correlation between NO₃⁻ and meteoric ¹⁰Be is widely applicable in
519 hyper-arid soils. However, as stated previously, NO₃⁻ and meteoric ¹⁰Be data are needed to ascertain the general
520 profile and slope behavior within the region. Additionally, though our NO₃⁻ estimated ages are validated using *in-*
521 *situ* data from previous studies, the NO₃⁻ dating tool will need to be further evaluated with additional measurements
522 and erosion, initial inventory, and inheritance corrections.

524 **6.1. Calculated, estimated, and inferred exposure age validation**

525 Considering the novelty of our approach, we sought to test and externally validate the exposure ages. Our
526 calculated, estimated, and inferred exposure ages are consistent with the limited *in-situ* exposure age data from the
527 Shackleton Glacier region (<http://antarctica.ice.d.org>; Balco, 2020). Exposure ages from glacial erratic boulders
528 using *in-situ* cosmogenic measurements were determined in previous studies (Balter-Kennedy et al., 2020; Balco,
529 2020; <http://antarctica.ice.d.org>) from Roberts Massif, Thanksgiving Valley, and Mt. Franke (Figs. 8 and 9). From
530 *in-situ* ¹⁰Be, ²⁶Al, ³He, and ²¹Ne data, exposure ages on the northern flank of Roberts Massif range from 1.10 Ma to
531 3.26 Ma (Balter-Kennedy et al., 2020; Balco, 2020; <http://antarctica.ice.d.org>), and our measured, estimated, and
532 inferred ages without erosion are 1.67 Ma, 1.74 Ma, and 1.94 Ma, respectively. Our ages, which are likely
533 overestimates due to a lack of initial inventory or inheritance corrections, are comparable to these nearby *in-situ*
534 ages at similar elevations (Figs. 8 and 9). The ages with the erosion term are greater and outside the range from
535 Balter-Kennedy et al. (2020). This suggests that soil erosion rates are probably low at Roberts Massif, and the initial
536 inventory and ¹⁰Be inheritance from previous exposures are likely significantly smaller than the measured inventory.
537 Otherwise, the corrected meteoric ¹⁰Be exposure ages would be much greater than the *in-situ* ages.

538 To the north, the *in-situ* ages from erratic boulders at Thanksgiving Valley vary greatly from ~4.3 ka near
539 the glacier to 450 ka at higher elevations, though most ages appear to be around 30 ka (Figs. 8 and 9) (Balco, 2020;
540 <http://antarctica.ice.d.org>). Our exposure ages are greater than most previous ages. In particular, the sample

541 collected closest to Shackleton Glacier has an inferred age two orders of magnitude higher than the *in situ* age from
542 a nearby glacial erratic at the same elevation (Fig. 9). Given the location (~100 m from the glacier) and young
543 nearby *in situ* age (~4.3 ka), this location was likely covered during the LGM and other glacial periods. Therefore,
544 considering the high surface concentration of meteoric ¹⁰Be for this sample, it is possible that there is an additional
545 delivery mechanism of ¹⁰Be, such as deposition of material deflated from the valley walls or at high elevations, or an
546 otherwise large inherited component.

547 Closer to the Ross Ice Shelf, the *in situ* ages from Mt. Franke range from ~29 ka to 220 ka. Our estimated
548 age without erosion is at the top that range at 220 ka, though the inferred ages are considerable younger at 94 ka and
549 72 ka (Table 5). Similar to Roberts Massif, our ages from Mt. Franke ages are comparable to the *in situ* ages from
550 similar elevations (Fig. 9). Here, soil erosion, initial inventory, and inheritance likely minimally influence the
551 measured ¹⁰Be inventory. We argue that while the measured, estimated, and inferred ages from the Shackleton
552 Glacier region are similar to *in situ* ages, they are likely an overestimate and most useful from a relative perspective
553 in understanding which surfaces have been exposed for longer than others.

554 6.2. NO₃⁻ as an efficient inventory and exposure age estimation tool

555 This is the first study to use NO₃⁻ concentrations to directly estimate meteoric ¹⁰Be concentrations study,
556 but not the first to attempt to use water-soluble NO₃⁻ and salts to help understand glacial history. Previous studies
557 have argued that atmosphere-derived salt concentrations at the surface may correlate with exposure ages and wetting
558 ages in Antarctica (Graham et al., 2002; Graly et al., 2018; Lyons et al., 2016; Schiller et al., 2009). Graly et al.
559 (2018) showed that, in particular, water-soluble NO₃⁻ and boron exhibited the strongest relationships with exposure
560 age ($R^2 = 0.9$ and 0.99 , respectively). Lyons et al. (2016) used nitrate concentrations to estimate the amount of time
561 since the soils were last wetted and Graham et al. (2002) attempted to calculate exposure ages using the inventory of
562 nitrate in the soil. Graly et al. (2018) argue that boron is preferable to nitrate due to concerns related to nitrate
563 mobility under sub-arid conditions (e.g. Frey et al., 2009; Michalski et al., 2005), and given that uncertainties in
564 local accumulation rates and ion transport can result in inaccurate ages when using NO₃⁻ alone (Graham et al., 2002;
565 Schiller et al., 2009). Based on the results presented here for hyper-arid CTAM ice-free regions and the concerns
566 with boron mobility depending on whether the B species present in the soils is BO₃²⁻ (borate) or H₃BO₃ (boric acid),
567 we conclude that NO₃⁻ appears suitable for relative age dating and for producing age estimates.

568 We show that the differences between measured ¹⁰Be inventories and estimated inventories using NO₃⁻ are
569 low (see Section 5.3.2) and argue that the power-law relationship between meteoric ¹⁰Be and NO₃⁻ can be used to
570 expand our current exposure age database for the TAM, compared to cosmogenic radionuclide analyses, NO₃⁻
571 analyses are rapid and cost-effective. However, a model using NO₃⁻ or salts alone is likely insufficient, unless the
572 anion-accumulation rates are known (Graham et al., 2002; Schiller et al., 2009). Though the regressions between
573 NO₃⁻ and ¹⁰Be are strong (Fig. 6c), each of the three profiles from Roberts Massif, Bennett Platform, and
574 Thanksgiving Valley have different regression coefficients and slopes. In other words, the nature of the relationship
575 between meteoric ¹⁰Be and NO₃⁻ varies across the Shackleton Glacier region and varies depending on the location.
576 This is likely due to differences in NO₃⁻ and ¹⁰Be transport and mobility in different surface environments and under
577 different local climates. To address these uncertainties, some ¹⁰Be data (surface samples for all locations and a few
578 depth profiles) are necessary to constrain the most accurate regression and minimize the associated error.

579 We tested our meteoric ¹⁰Be—NO₃⁻ model with data from Arena Valley in the MDV (Graham et al., 2002)
580 and found that our model is applicable to other TAM ice-free areas. Similar to the Shackleton Glacier region soils,
581 the soils from Arena Valley are hyper-arid with high concentrations of NO₃⁻ and other salts (Graham et al., 2002).
582 Precipitation in the MDV is low at ~5 cm water equivalent each year (Fountain et al., 1999), though NO₃⁻ and other
583 water-soluble salts at the surface can be wetted and mobilized. The highest NO₃⁻ concentrations are at 10 cm depth,
584 while ¹⁰Be concentrations are highest at the surface and decrease with depth, indicating vertical transport of NO₃⁻
585 through time (Graham et al., 2002). The power-law relationship between ¹⁰Be and NO₃⁻ throughout the profile is
586 weaker for the Arena Valley samples compared to Shackleton Glacier samples; there is a stronger power-law

587 correlation in the top 20 cm ($R^2 = 0.61$) compared to the bottom 70 cm ($R^2 < 0.01$), though the profile is
588 considerably deeper (110 cm). Using the power-law relationship from Bennett Platform, which mostly closely
589 resembles the profile behavior for Arena Valley given the negative regression slope, the estimated inventory is $5.4 \times$
590 10^{10} atoms. The measured inventory is of the same order of magnitude, 1.3×10^{10} atoms, indicating a moderate
591 model fit. Applying the power-law relationship from Arena Valley, the estimated inventory is 9.2×10^8 atoms,
592 which is ~27% lower than the measured inventory. These results indicate that, although the Shackleton Glacier
593 region is nearly 900 km from Arena Valley, the correlation between NO_3^- and meteoric ^{10}Be is widely applicable in
594 hyper-arid soils. However, as stated previously, NO_3^- and meteoric ^{10}Be data are needed to ascertain the general
595 profile and slope behavior within the region. Additionally, though our NO_3^- estimated ages are validated using *in-*
596 *situ* data from previous studies, the NO_3^- dating tool will need to be further evaluated with additional measurements
597 and erosion, initial inventory, and inheritance corrections.

598 6.3. Implications for paleoclimate and ice sheet dynamics

599 Our work demonstrates that NO_3^- and ^{10}Be are correlated in much of the Shackleton Glacier region, and the
600 soil profiles can inform our understanding of surficial processes and soil wetting for the region, and this relationship
601 has important implications for understanding landscape disturbance, either by meltwater or glacier overriding.
602 Exposure age and cosmogenic nuclide data from across Antarctica show that a polar desert regime began in the mid-
603 Miocene and has persisted into modern time (Lewis et al., 2008; Marchant et al., 1996; Spector and Balco, 2020;
604 Valletta et al., 2015). Additionally, Barrett (2013) provides a detailed review of studies focused on Antarctic glacial
605 history, particularly centered around the “stabilist vs. dynamicist” debate concerning the overall stability of the
606 EAIS. Interpreting 40+ years of data from published literature, they conclude that the EAIS is stable in the interior
607 with retreat occurring along the margins, including at outlet glaciers (Golledge et al., 2012). Given these findings,
608 we would expect NO_3^- and meteoric ^{10}Be concentrations to be ~~correlated~~ correlated in hyper-arid Antarctic soils,
609 such as those from the Shackleton Glacier region, as both constituents are derived from atmospheric deposition with
610 minimal alteration at the surface. The major differences between the two concern transport mechanisms: ~~in-~~
611 Meteoric ^{10}Be transport is limited by clay particle mobility and NO_3^- is mobile upon soil wetting. ~~Deviations in the~~
612 ~~expected relationship between ^{10}Be and NO_3^- can inform knowledge of surface processes in the TAM.~~

613 If we assume an “ideal” situation where an undisturbed hyper-arid soil has accumulated meteoric ^{10}Be (Fig.
614 3a-b), ^{10}Be concentrations would be highest at the surface and eventually decrease to background levels at depth.
615 None of the profiles we sampled and measured for meteoric ^{10}Be and NO_3^- reached background concentrations. All
616 profiles were sampled until frozen soil was reached (or bedrock at Schroeder Hill) (Fig. S16), demonstrating had an
617 active layer much shallower than those from the MDV (Graham et al., 2002; Schiller et al., 2009; Valletta et al.,
618 2015). This suggests that the active layer may have deepened and shallowed throughout time, and modern ^{10}Be -
619 laden particles were able to migrate deeper in the past and mobility has been relatively recently (within the ^{10}Be
620 half-life)s limited to the top ~20 cm for most of the Shackleton Glacier region. Though clay particle translocation
621 by percolating water can explain the correlated behavior of ^{10}Be and NO_3^- at Roberts Massif and Thanksgiving
622 Valley, it is unlikely that the region had sufficient precipitation for significant percolation over the last 14 Ma, given
623 the high NO_3^- concentrations (Menziés et al., 2006). The concentrations of fine particles in the soil profiles also do
624 not change significantly with depth, as would be expected if large precipitation or melt events were frequent (Fig. 4).
625 Additionally, the soils horizons are moderately well defined (Fig. 4), suggesting minimal cryoturbation.

626 Similar to Arena Valley and Wright Valley in the MDV (Graham et al., 2002; Schiller et al., 2009), NO_3^-
627 concentrations are highest just beneath the surface at Roberts Massif, indicating shallow salt migration under an arid
628 climate. These data suggest that the samples furthest inland at Roberts Massif and Thanksgiving Valley have been
629 fairly undisturbed since at least the middle to late Pleistocene, given the soil exposure age estimates of exposure
630 duration (see Section 6.2). ~~Although~~ Since meteoric ^{10}Be and NO_3^- at Bennett Platform are mirrored with a negative
631 power-law slope, we argue that the difference could be due to 1) additional ^{10}Be delivery or 2) enhanced NO_3^-
632 transport, is not due to NO_3^- mobility, but instead ^{10}Be deposition. Bennett Platform was the only location we
633 sampled on a large moraine (Fig. 2c), and as such, we would expect minimal inheritance with a constructional

634 landform we would expect ¹⁰Be to be highest at the surface and decrease to background concentrations decreasing at
635 depth. This is generally the observed behavior, with significantly higher surface concentrations. The NO₃⁻ profile
636 behavior is similar to those throughout the Shackleton Glacier region, though the concentrations continue to increase
637 with depth, possibly indicating minor-some percolation of NO₃⁻ rich brine. What may be considered the
638 “anomalous” data point is the surface concentration of meteoric ¹⁰Be. Even though we sampled a constructional
639 landform, the sample was collected between two boulder lines in a small, local depression (~1 m) (Table 2). It is
640 probably no coincidence that this location also has the greatest proportion of fine-grained material in the soil profile.
641 The two boulder lines impede wind flow and act as a sediment and snow trap, possibly resulting in a higher
642 concentration of meteoric ¹⁰Be than expected simply from atmospheric deposition. The snow in the depression may
643 also aid in NO₃⁻ transport when melted. In this case, an additional sediment-laden ¹⁰Be deposition term (superseding
644 any erosion) and/or possible salt transport needs to be considered to accurately date the moraine, and the current
645 exposure age we measured may be an overestimate.

646 **6.2. Attempt at inferring ed-surface exposure duration approximation and thoughts on glacial history**

647 We used the relationship between the maximum meteoric ¹⁰Be concentration in the soil profile and the
648 meteoric ¹⁰Be inventory (Graly et al., 2010) to “infer” speculatively infer ¹⁰Be inventories and estimate maximum
649 exposure durations for all eleven locations with and without erosion using Eq. 5 (Fig. 7; Table 3). As is the case for
650 Roberts Massif and Thanksgiving Valley, the highest ¹⁰Be concentrations may not always be at the surface for all
651 locations; however, the relationship is sufficiently strong to provide an estimate of the ¹⁰Be inventory and thus an
652 exposure duration estimate.

$$653 t = -\frac{1}{\lambda} \cdot \ln \left[1 - \frac{\lambda I}{Q - E\rho N} \right] \quad (5)$$

654 We did not measure erosion rates in this study. Balter-Kennedy et al. (2020) determined that erosion rates
655 for boulders at Roberts Massif which were less than 2 cm Ma⁻¹. Considering we are investigating soils, we chose a
656 conservative value of 5 cm Ma⁻¹ for our calculations. We chose a ¹⁰Be flux value (Q) of 1.3 x 10⁵ atoms cm⁻² yr⁻¹
657 from Taylor Dome (Steig et al., 1995) due to a similar climate to that of the CTAM and an absence of local meteoric
658 ¹⁰Be flux data.

659 Compared to the measured inventories from Roberts Massif, Bennett Platform, and Thanksgiving Valley
660 (from the ¹⁰Be depth profiles; see Section 5.1), the inferred inventories differ by ~16-130%. The inferred exposure
661 estimates with erosion range from 58 ka to >6.5 Ma, and the estimates without erosion range from 57 ka to 1.94 Ma
662 for Mt. Speed and Roberts Massif, respectively (Fig 8; Table 3). With the exception of Roberts Massif,
663 Thanksgiving Valley, and Mt. Speed, the oldest surfaces are those which we sampled furthest from the glacier,
664 which is consistent with our sampling methodology to capture younger and older soils. The sample from Roberts
665 Massif collected closest to the glacier has an estimated exposure duration that is outside the model limits (>6.5 Ma).

Formatted: Font: Bold

Formatted: Heading 2, Indent: First line: 0", Line spacing: Multiple 1.15 li

Formatted: Line spacing: Multiple 1.15 li

Formatted: Indent: First line: 0", Line spacing: Multiple 1.15 li, Tab stops: 6", Left

Formatted: Line spacing: Multiple 1.15 li

666 The youngest surfaces we sampled [from the Shackleton Glacier region](#) are those from the lowest elevations
667 and closest to the Ross Ice Shelf (Fig. 408). This is generally consistent with previous glacial modeling studies
668 which show that the greatest fluctuations in glacier height during the LGM were along outlet glacier and ice shelf
669 margins (Golledge et al., 2012; Mackintosh et al., 2011, 2014). ~~However, erosion rates are low throughout~~
670 ~~Antarctica (Balter Kennedy et al., 2020; Ivy-Ochs et al., 1995; Morgan et al., 2010) and would not drastically~~
671 ~~impact our relatively young inferred ages (Fig. 10). Additionally, background concentrations of meteoric ¹⁰Be in~~
672 ~~other Antarctic soil profiles are often approximately one to two order of magnitude lower than surface~~
673 ~~concentrations (Fig. 6). With these considerations~~Given the low erosion rates throughout Antarctica (Balter-
674 Kennedy et al., 2020; Ivy-Ochs et al., 1995; Morgan et al., 2010) and possibly low background concentrations of
675 meteoric ¹⁰Be (Dickinson et al., 2012; Schiller et al., 2009; Valletta et al., 2015), the Mt. Speed, Mt. Wasko, and Mt.
676 Franke samples were all likely covered by the Shackleton Glacier during the LGM, as well as the lower elevation,
677 ~~closest to the near-~~glacier samples from Mt. Heekin, Bennett Platform, and Mt. Augustana. The ~~samples we~~
678 ~~collected near the head of Shackleton Glacier encompass a range of ages, where lower elevation soils are relatively~~
679 ~~younger, though the~~ soils from Schroeder Hill and Roberts Massif have likely been exposed since the early
680 Pleistocene (Fig. 408). We also attempted to estimate exposure durations using two additional methods: 1) the
681 measured ¹⁰Be inventories for Roberts Massif, Bennett Platform, and Thanksgiving Valley, and 2) by calculating
682 ¹⁰Be concentrations using regressions of NO₃⁻ and ¹⁰Be for all seven locations with depth profiles, as detailed in the
683 supplementary materials. These exposure estimates are similar and range from ~100 ka at Bennet Platform to <4.5
684 Ma at Roberts Massif (Fig. S4; Table S3).

685 Sirius Group deposits were observed at Roberts Massif and were deposited as the Shackleton Glacier
686 retreated in this region (Fig. 2a). Evidence for a dynamic EAIS is derived primarily from the diamictite rocks (tills)
687 of the Sirius Group, which are found throughout the TAM and include well-documented outcrops in the Shackleton
688 Glacier region, but their age is unknown (Hambrey et al., 2003). Some of the deposits contain pieces of shrubby
689 vegetation, suggesting that the Sirius Group formed under conditions warmer than present with ~~woody trees~~ plants
690 occupying inland portions of Antarctica (Webb et al., 1984, 1996; Webb and Harwood, 1991). Sparse marine
691 diatoms found in the sediments were initially interpreted as evidence for the formation of the Sirius Group via
692 glacial over riding of the TAM during the warmer Pliocene (Barrett et al., 1992), though it is now argued that the
693 marine diatoms were wind-derived contamination, indicating that the Sirius Group is older (Scherer et al., 2016;

694 Stroeven et al., 1996). We document a large diamictite at site RM2-8 that is underlain by soils with an inferred ~~age~~
695 ~~exposure~~ of at least 1.9 Ma, possibly greater than 6.5 Ma. These exposure ~~ages-duration estimates~~ suggest that the
696 loose Sirius Group diamict was deposited at Roberts Massif some point after the Pliocene. While these data cannot
697 constrain the age of the formation, we suggest that the diamict could have formed prior to the Pliocene and was
698 transported during the Pleistocene glaciations.

699 7. Conclusions

700 We ~~measured-determined~~ concentrations of meteoric ^{10}Be and NO_3^- in soils from eleven ice-free areas
701 along the Shackleton Glacier, Antarctica, which ~~include-are among~~ the highest measured meteoric ^{10}Be
702 concentrations from the polar regions. ~~Concentrations of meteoric ^{10}Be spanned from 1.9×10^8 atoms g^{-1} at Bennett~~
703 ~~Platform to 73×10^8 atoms g^{-1} at Roberts Massif. The concentrations of NO_3^- were similarly variable and ranged~~
704 ~~from $\sim 1 \mu\text{g g}^{-1}$ near the ice shelf to 15mg g^{-1} near the Polar Plateau. In general, the lowest concentrations of ^{10}Be~~
705 ~~and NO_3^- we measured were at low elevations, near the ice shelf, and closest to the glacier. Measured (using~~
706 ~~meteoric ^{10}Be inventories), estimated (using the power-law relationship between NO_3^- and ^{10}Be), and inferred (using~~
707 ~~the relationship between maximum ^{10}Be and total inventory) exposure ages were calculated and ranged from 58 ka~~
708 ~~to >6.5 Ma with an estimated erosion component and 57 ka to 1.9 Ma without erosion. In general, there is good~~
709 ~~agreement between the three techniques.~~

710 The estimated and inferred ages without erosion at Roberts Massif, Thanksgiving Valley, and Mt. Frank are
711 similar to nearby *in-situ* ages from previous studies. In particular, relating NO_3^- concentrations to ^{10}Be
712 measurements results an efficient method to attain a greater number of exposure ages in the CTAM, a region with
713 currently sparse meteoric ^{10}Be data. However, the power-law relationship between NO_3^- and ^{10}Be had either a
714 positive or negative slope depending on the location, therefore the widespread applicability of this tool needs to be
715 further evaluated. Additionally, though we assumed an erosion rate for the region, some soils in local topographic
716 lows probably have a positive particle flux.

717 Since NO_3^- and ^{10}Be are both derived from atmospheric deposition, we expect the shape of their
718 accumulation profiles to be similar at depth in hyper-arid soils. In general, this was true for Roberts Massif and
719 Thanksgiving Valley, while NO_3^- and ^{10}Be concentrations were mirrored at Bennett Platform. We conclude that
720 much of the southern Shackleton Glacier region has maintained persistent arid conditions since at least the

721 Pleistocene, though the region ~~was may have been~~ warmer and wetter in the past, as evidenced ~~by by frozen soil at~~
722 ~~the bottom of our depth profiles~~ the Sirius Group diamict. The onset of aridity is particularly important in
723 understanding refugia and ecological succession in TAM soils. Since the ~~parts of the~~ region ~~haves~~ remained hyper-
724 arid and undisturbed for upwards of a few million years, prolonged exposure has resulted in the accumulation of
725 salts at high concentrations in the soils. ~~As such, it~~ is an enigma how soil organisms have persisted throughout
726 glacial-interglacial cycles. However, it is possible that organisms have survived near the glacier at locations like Mt.
727 Augustana, where glacial advance appears to have been minimal during the LGM, but seasonal summer melt has the
728 potential to solubilize salts.

729 Overall, our data show that the relatively youngest soils we sampled were at lower elevations near the
730 Shackleton Glacier terminus and lower elevations further inland (typically near the glacier). ~~Inferred estimates range~~
731 ~~from 57 ka (though likely post LGM when corrected) to 1.94 Ma, possibly >6.5 Ma with erosion.~~ Our sampling
732 scheme was successful in capturing a range of surface exposure ~~ages~~ durations which ~~can~~ contribute to growing
733 archives in the CTAM. ~~There are outstanding issues regarding inheritance dynamics of meteoric ¹⁰Be in disturbed~~
734 ~~environments, and particle erosion/deposition rates, and NO₃⁻ mobility.~~ We hope that future studies will ~~further~~
735 ~~evaluate the relationship between water-soluble salts (e.g., NO₃⁻) and meteoric ¹⁰Be as a proxies for landscape~~
736 ~~disturbance and exposure age.~~ ~~address the outstanding issues regarding inheritance dynamics of meteoric-¹⁰Be in~~
737 ~~disturbed environments and particle erosion/deposition rates.~~

738

739 **Author Contributions**

740 The project was designed and funded by BJA, DHW, IDH, NF, and WBL. Fieldwork was conducted by BJA, DHW,
741 IDH, NF, and MAD. LBC, PRB, and MAD prepared the samples for meteoric ^{10}Be analysis and MAD analyzed the
742 samples for NO_3^- . MAD wrote the article with contributions and edits from all authors.

743 **Data Availability Statement**

744 The datasets generated for this study are included in the article or supplementary materials.

745 **Competing Interests**

746 The authors declare that they have no conflict of interest.

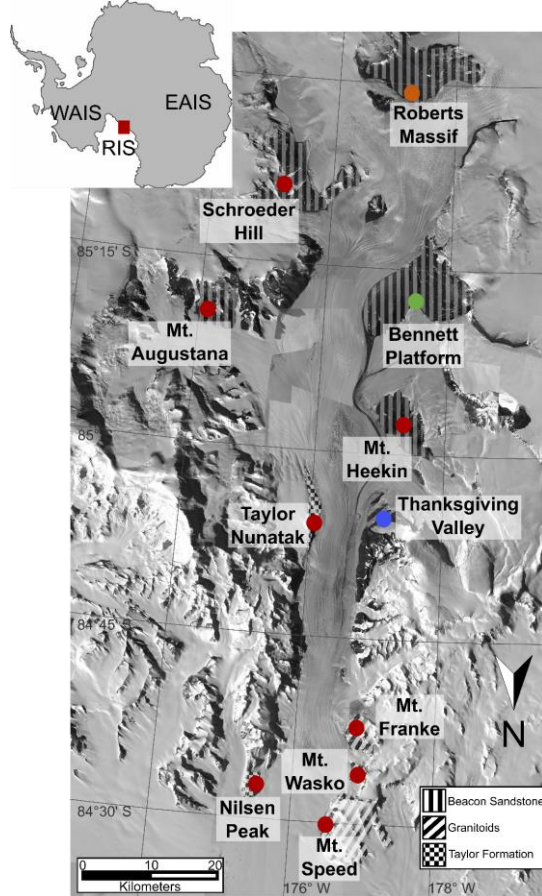
747 **Acknowledgments**

748 We thank the United States Antarctic Program (USAP), Antarctic Science Contractors (ASC), Petroleum
749 Helicopters Inc. (PHI), and Marci Shaver-Adams for logistical and field support. We especially thank Dr. Marc
750 Caffè and the Purdue University PRIME Lab for their assistance with AMS measurements. Additionally, we thank
751 Dr. Andrew Christ at University of Vermont for thoughtful discussions and Dr. Sue Welch and Daniel Gilbert at The
752 Ohio State University for help with initial laboratory analyses. We appreciate the detailed and thoughtful
753 suggestions and edits from Dr. Brent Goehring and an anonymous reviewer which have greatly improved this
754 manuscript. This work was supported by NSF OPP grants 1341631 (WBL), 1341618 (DHW), 1341629 (NF),
755 1341736 (BJA), NSF GRFP fellowship 60041697 (MAD), and a PRIME Lab seed proposal (MAD). Sample
756 preparation and LBC's time supported by NSF EAR 1735676. Geospatial support for this work provided by the
757 Polar Geospatial Center under NSF OPP grants 1043681 and 1559691.

758

759 **Figures:**

760 **Figure 1:** Overview map of the Shackleton Glacier region, located in the Queen Maud Mountains of the Central
761 Transantarctic Mountains. The red circles represent our eleven sampling locations, with an emphasis on Roberts
762 Massif (orange), Bennett Platform (green), and Thanksgiving Valley (blue), which have the most comprehensive
763 dataset in this study. The bedrock serves as primary weathering product for soil formation (Elliot and Fanning, 2008;
764 Paulsen et al., 2004). Base maps provided by the Polar Geospatial Center.

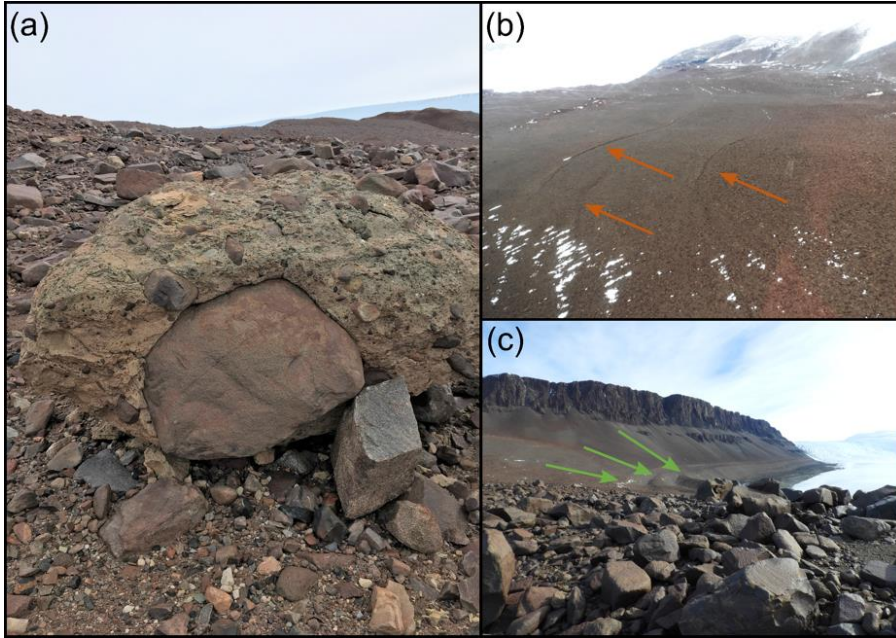


765

766

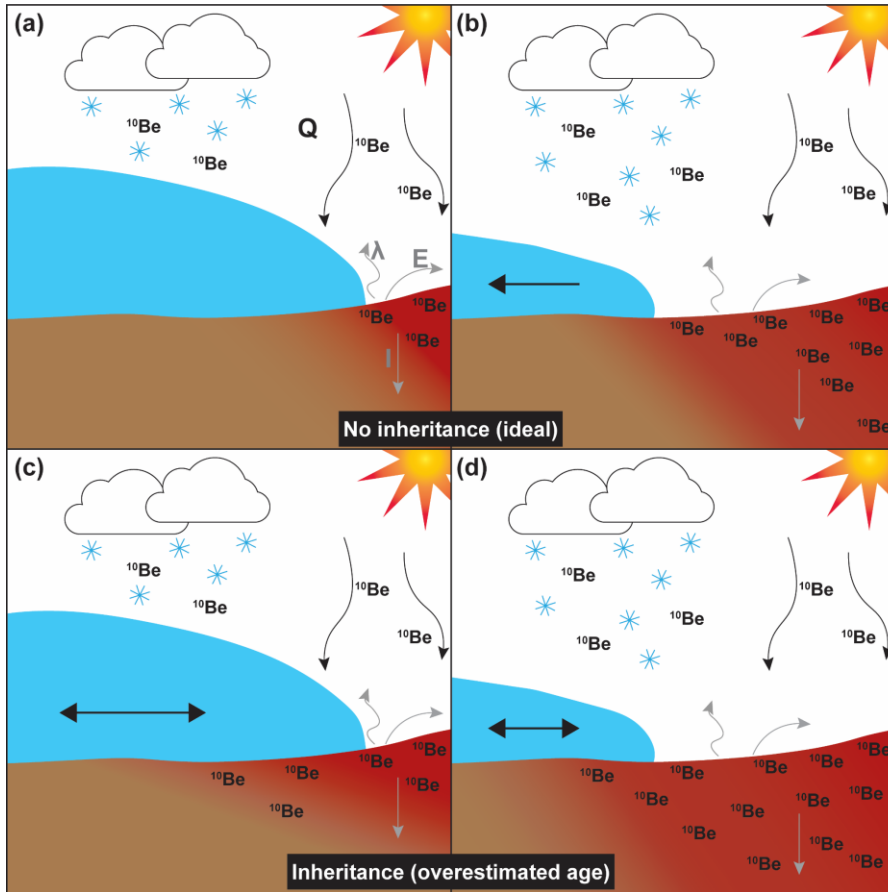
767

768 **Figure 2:** The Sirius Group was documented at Roberts Massif near the RM2-8 sampling location (a). Small
769 moraines were observed at Roberts Massif (b) and large moraines at Bennett Platform (c).
770



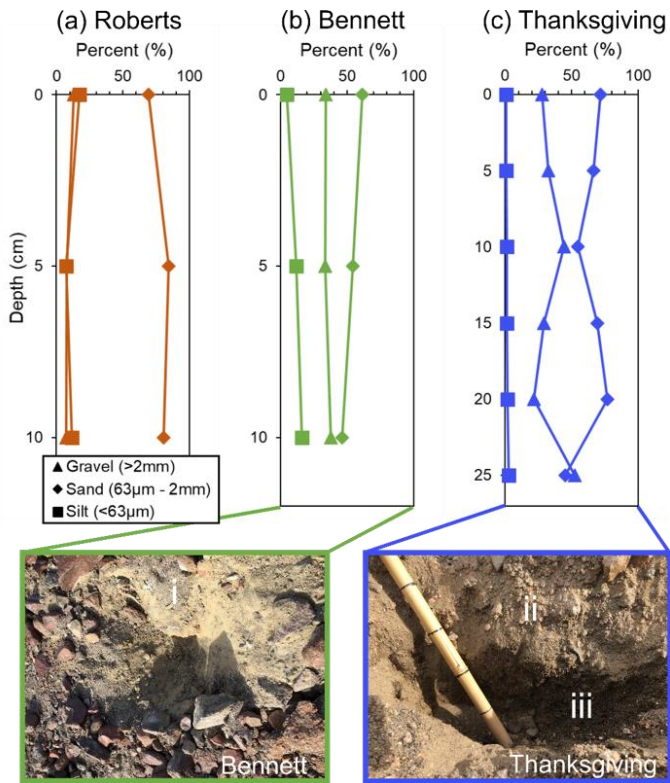
771

772 **Figure 3:** Conceptual diagram of meteoric ^{10}Be accumulation in soils during glacial advance and retreat. In “ideal”
 773 conditions, ^{10}Be accumulates in exposed soils and ^{10}Be concentrations beneath the glacier are negligible at
 774 background levels (a). As the glacier retreats, ^{10}Be can begin accumulating in the recently exposed soil and an
 775 inventory can be measured to calculate exposure agesduration. In the case where the glacier has waxed and waned
 776 numerous times and the soils already contain a non-negligible “inheritance” concentration of ^{10}Be , the inventories
 777 would need to be corrected for ^{10}Be inheritance (c-d) to accurately determine exposure agesduration.
 778



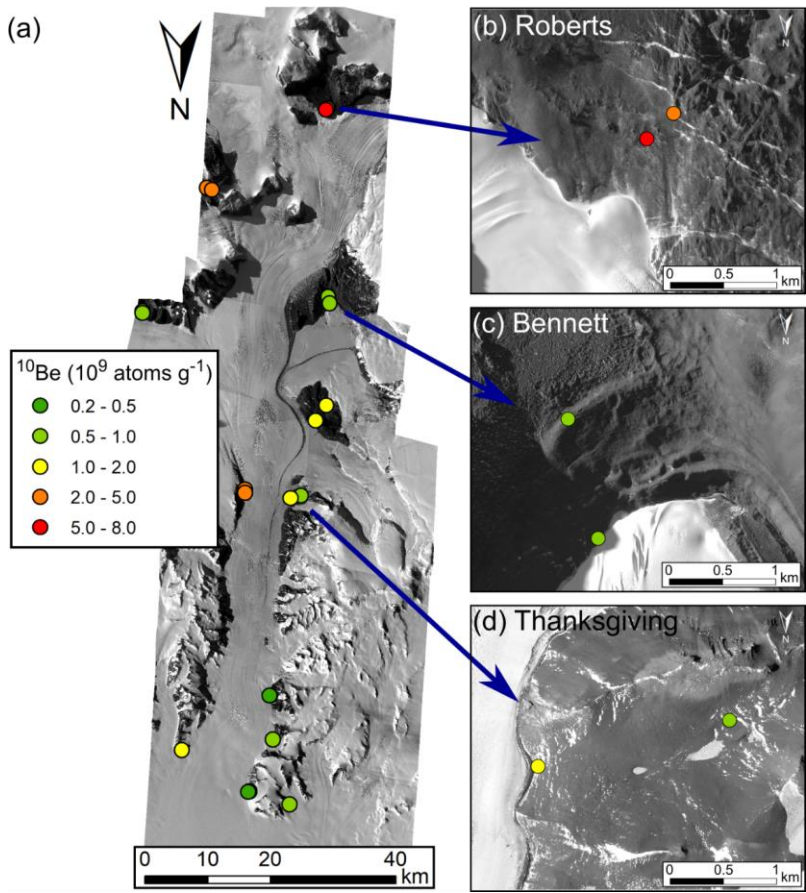
779

780 **Figure 4:** The grain size composition of soil profiles collected from Roberts Massif (a, orange), Bennett Platform (b,
 781 green), and Thanksgiving Valley (c, blue). The soil pits from Bennett Platform and Thanksgiving Valley are also
 782 shown with distinct soil horizons.
 783



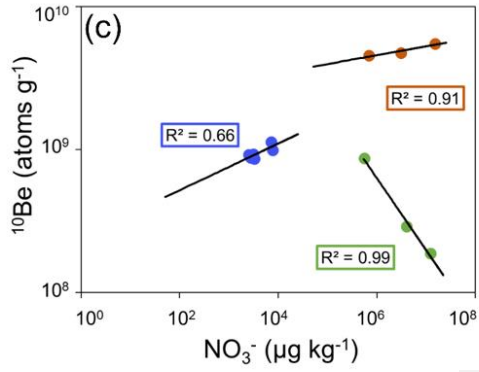
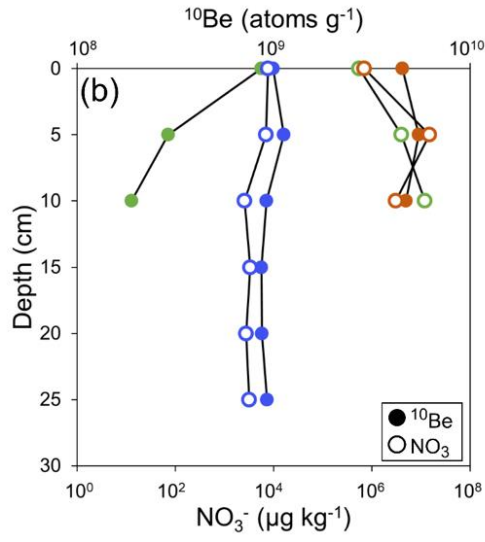
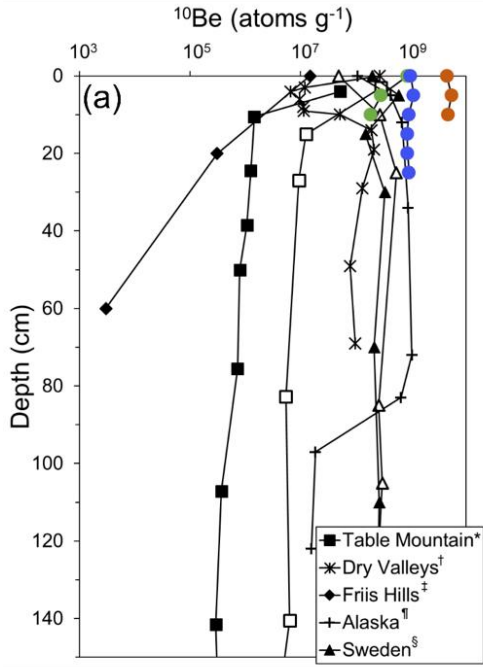
784

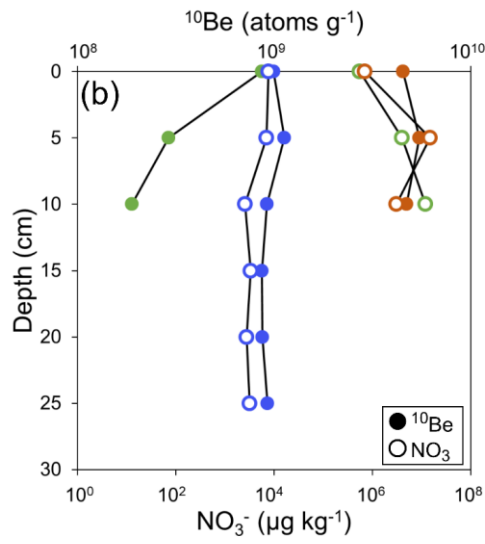
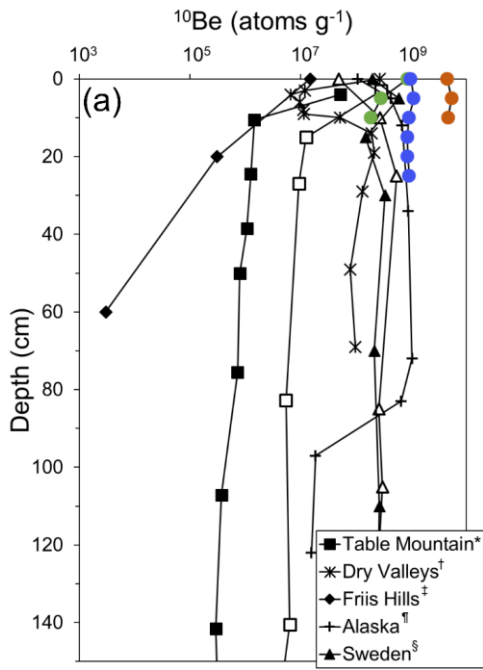
785 **Figure 5:** Spatial distribution of surface meteoric ^{10}Be concentrations in the Shackleton Glacier region (a). Where
786 possible, two samples were collected at each location to represent surfaces closest to the glacier, which might have
787 been glaciated during recent glacial periods, and samples furthest from the glacier that are likely to have been
788 exposed during recent glacial periods. Insets of Roberts Massif (b), Bennett Platform (c), and Thanksgiving Valley
789 (d) are included, as these locations serve [as the basis for our relative exposure age models](#) [have both \$^{10}\text{Be}\$ and \$\text{NO}_3^-\$](#)
790 [depth profile data](#). Base maps [were](#) provided by the Polar Geospatial Center.
791



792

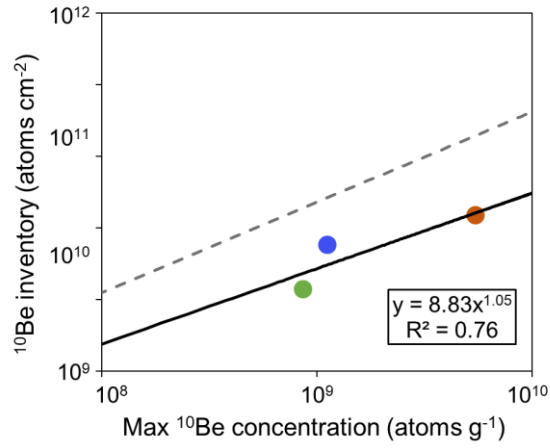
793 **Figure 6:** Soil profiles of meteoric ^{10}Be concentrations for Roberts Massif (orange), Bennett Platform (green), and
794 Thanksgiving Valley (blue) compared to profiles from the Antarctic (Dickinson et al., 2012⁷; Schiller et al., 2009¹;
795 Valletta et al., 2015²) and Arctic (Bierman et al., 2014⁴; Ebert et al., 2012⁸) (a). The ^{10}Be concentration profiles were
796 also compared to NO_3^- concentration profiles (b) ~~and a power function was fit to the data (c).~~
797





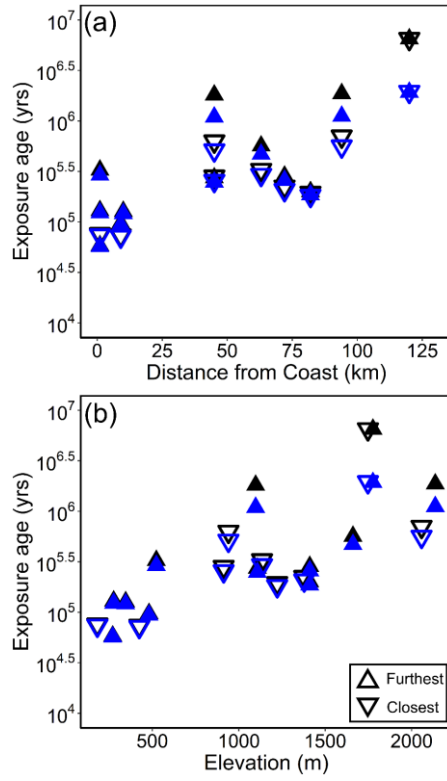
800
801

802 **Figure 7:** Relationship between the measured maximum (or surface) meteoric ^{10}Be concentration and the calculated
803 inventory (Eq. 2). This relationship is used to infer ^{10}Be inventories given a maximum or surface concentration
804 (Graly et al., 2010). The solid black line is the power relationship between concentration and inventory, while the
805 dashed grey line is the regression from Graly et al. (2010).
806



807
808

809 **Figure 8:** Inferred surface exposure durations versus distance from the coast (a) and elevation (b), with (black) and
810 without (blue) an assumed erosion term. Upward facing triangles are samples collected furthest from the glacier,
811 while downward triangles are samples collected closest to the glacier.



Formatted: Normal, Centered

Formatted: Font: 12 pt, Not Bold

812

813
814
815

Table 1: Concentrations of meteoric ^{10}Be and water-soluble nitrate (NO_3^-) in Shackleton Glacier region surface soils and depth profiles. Additional information on ^{10}Be corrections is located in Table S2.

<u>Sample Name</u>	<u>Location</u>	<u>Latitude</u>	<u>Longitude</u>	<u>Elevation (m)</u>	<u>Distance from Coast (km)</u>	<u>Depth (cm)</u>	<u>^{10}Be Concentration (10^9 atoms g^{-1})</u>	<u>NO_3^- Concentration (10^5 $\mu\text{g kg}^{-1}$)</u>
AV2-1	Mt. Augustana	-85.1706	-174.1338	1410	72	0-5	1.162	7.77
AV2-1	Mt. Augustana	-85.1706	-174.1338	1410	72	5-10	-	12.2
AV2-1	Mt. Augustana	-85.1706	-174.1338	1410	72	10-15	-	13.4
AV2-8	Mt. Augustana	-85.1676	-174.1393	1378	72	0-5	0.955	-
BP2-1	Bennett Platform	-85.2121	-177.3576	1410	82	0-5	0.868	5.57
BP2-1	Bennett Platform	-85.2121	-177.3576	1410	82	5-10	0.291	39.8
BP2-1	Bennett Platform	-85.2121	-177.3576	1410	82	10-15	0.188	121
BP2-8	Bennett Platform	-85.2024	-177.3907	1222	82	0-5	0.848	-
MF2-1	Mt. Franke	-84.6236	-176.7353	480	9	0-5	0.462	0.041
MF2-1	Mt. Franke	-84.6236	-176.7353	480	9	5-10	-	0.014
MF2-1	Mt. Franke	-84.6236	-176.7353	480	9	10-15	-	0.010
MF2-1	Mt. Franke	-84.6236	-176.7353	480	9	15-20	-	0.011
MF2-4	Mt. Franke	-84.6237	-176.7252	424	9	0-5	0.360	-
MH2-1	Mt. Heekin	-85.0299	-177.2405	1098	63	0-5	1.956	18.0
MH2-1	Mt. Heekin	-85.0299	-177.2405	1098	63	5-10	-	27.4
MH2-1	Mt. Heekin	-85.0299	-177.2405	1098	63	10-15	-	18.8
MH2-8	Mt. Heekin	-85.0528	-177.4099	1209	63	0-5	1.300	-
MSP2-1	Mt. Speed	-84.4819	-176.5070	270	0	0-5	0.291	-
MSP2-4	Mt. Speed	-84.4811	-176.4864	181	0	0-5	0.370	-
MSP4-1	Mt. Speed	-84.4661	-177.1224	276	0	0-5	0.596	-
MW4-1	Mt. Wasiko	-84.5600	-176.8177	345	10	0-5	0.586	-
NP2-5	Nilsen Peak	-84.6227	-176.7501	522	0	0-5	1.295	-
RM2-1	Roberts Massif	-85.4879	-177.1844	1776	120	0-5	4.538	6.94
RM2-1	Roberts Massif	-85.4879	-177.1844	1776	120	5-10	5.475	149
RM2-1	Roberts Massif	-85.4879	-177.1844	1776	120	10-15	4.721	30.7
RM2-8	Roberts Massif	-85.4857	-177.1549	1747	120	0-5	7.327	-
SH3-2	Schroeder Hill	-85.3597	-175.0693	2137	94	0-5	3.850	75.5
SH3-2	Schroeder Hill	-85.3597	-175.0693	2137	94	5-10	-	16.1

<u>SH3-2</u>	<u>Schroeder Hill</u>	<u>-85.3597</u>	<u>-175.0693</u>	<u>2137</u>	<u>94</u>	<u>10-15</u>	<u>-</u>	<u>41.6</u>
<u>SH3-8</u>	<u>Schroeder Hill</u>	<u>-85.3569</u>	<u>-175.1621</u>	<u>2057</u>	<u>94</u>	<u>0-5</u>	<u>2.267</u>	<u>-</u>
<u>TGV2-1</u>	<u>Thanksgiving Valley</u>	<u>-84.9190</u>	<u>-177.0603</u>	<u>1107</u>	<u>45</u>	<u>0-5</u>	<u>0.993</u>	<u>0.077</u>
<u>TGV2-1</u>	<u>Thanksgiving Valley</u>	<u>-84.9190</u>	<u>-177.0603</u>	<u>1107</u>	<u>45</u>	<u>5-10</u>	<u>1.125</u>	<u>0.071</u>
<u>TGV2-1</u>	<u>Thanksgiving Valley</u>	<u>-84.9190</u>	<u>-177.0603</u>	<u>1107</u>	<u>45</u>	<u>10-15</u>	<u>0.921</u>	<u>0.025</u>
<u>TGV2-1</u>	<u>Thanksgiving Valley</u>	<u>-84.9190</u>	<u>-177.0603</u>	<u>1107</u>	<u>45</u>	<u>15-20</u>	<u>0.864</u>	<u>0.033</u>
<u>TGV2-1</u>	<u>Thanksgiving Valley</u>	<u>-84.9190</u>	<u>-177.0603</u>	<u>1107</u>	<u>45</u>	<u>20-25</u>	<u>0.874</u>	<u>0.028</u>
<u>TGV2-1</u>	<u>Thanksgiving Valley</u>	<u>-84.9190</u>	<u>-177.0603</u>	<u>1107</u>	<u>45</u>	<u>25-30</u>	<u>0.925</u>	<u>0.031</u>
<u>TGV2-8</u>	<u>Thanksgiving Valley</u>	<u>-84.9145</u>	<u>-176.8860</u>	<u>912</u>	<u>45</u>	<u>0-5</u>	<u>1.152</u>	<u>-</u>
<u>TN3-1</u>	<u>Taylor Nunatak</u>	<u>-84.9227</u>	<u>-176.1242</u>	<u>1097</u>	<u>45</u>	<u>0-5</u>	<u>3.802</u>	<u>-</u>
<u>TN3-5</u>	<u>Taylor Nunatak</u>	<u>-84.9182</u>	<u>-176.1282</u>	<u>940</u>	<u>45</u>	<u>0-5</u>	<u>2.105</u>	

817
818

Table 2: Surface features of the sample locations from the Shackleton Glacier region.

<u>Location</u>	<u>Sample name</u>	<u>Sample description</u>
<u>Mt. Augustana</u>	<u>AV2-1</u>	<u>Up valley from Gallup Glacier (tributary glacier); at valley floor: surface covered by cobbles and pebbles; red-stained sandstones nearby; frozen ground at bottom of depth profile</u>
<u>Mt. Augustana</u>	<u>AV2-8</u>	<u>At toe of Gallup Glacier; surface covered primarily by boulders; mainly sand between boulders</u>
<u>Bennett Platform</u>	<u>BP2-1</u>	<u>On larger moraine; local depression between two boulder lines, up valley from McGregor Glacier (tributary glacier); at valley floor</u>
<u>Bennett Platform</u>	<u>BP2-8</u>	<u>At toe of McGregor Glacier (tributary glacier); surface covered primarily by boulders; mainly sand between boulders</u>
<u>Mt. Franke</u>	<u>MF2-1</u>	<u>Bottom of wide valley floor; near small moraine; frozen soil at bottom of depth profile</u>
<u>Mt. Franke</u>	<u>MF2-4</u>	<u>Bottom of wide valley floor; near small moraine</u>
<u>Mt. Heekin</u>	<u>MH2-1</u>	<u>On high-elevation saddle; surface covered by sparse small boulders, cobbles, and pebbles; poorly consolidated till; frozen ground at bottom of profile</u>
<u>Mt. Heekin</u>	<u>MH2-8</u>	<u>At toe of Baldwin Glacier (alpine glacier) on valley floor; two ponds nearby; surface covered by loose rocks and sand; poorly consolidated till; possible polygonal surface nearby</u>
<u>Mt. Speed</u>	<u>MSP2-1</u>	<u>Steep slope; large granite boulders; scree</u>
<u>Mt. Speed</u>	<u>MSP2-4</u>	<u>Near cliff by Shackleton Glacier; large granite boulders; scree</u>
<u>Mt. Speed</u>	<u>MSP4-1</u>	<u>Spur on level with glacier; frozen soil near 5 cm depth</u>
<u>Mt. Wasko</u>	<u>MW4-1</u>	<u>Steep slope; large granite boulders; scree; nearby snowpack</u>
<u>Nilsen Peak</u>	<u>NP2-5</u>	<u>On ridge; near large snow patch</u>
<u>Roberts Massif</u>	<u>RM2-1</u>	<u>Near thin moraine; red-stained sandstones nearby with etches; frozen ground at bottom of depth profile</u>
<u>Roberts Massif</u>	<u>RM2-8</u>	<u>Near thin moraine and Sirius Group diamict; large boulders nearby with unconsolidated sediment</u>
<u>Schroeder Hill</u>	<u>SH3-2</u>	<u>Red-stained sandstone; poorly consolidated till; bedrock at bottom of profile</u>
<u>Schroeder Hill</u>	<u>SH3-8</u>	<u>Red-stained sandstone; poorly consolidated till;</u>
<u>Thanksgiving Valley</u>	<u>TGV2-1</u>	<u>Lightly uphill on valley wall; poorly consolidated till; frozen ground at bottom of depth profile; polygonal surface nearby</u>
<u>Thanksgiving Valley</u>	<u>TGV2-8</u>	<u>At the toe of Shackleton Glacier; near thin moraines, surface covered primarily large boulders</u>
<u>Taylor Nunatak</u>	<u>TN3-1</u>	<u>On ridge; surface covered by small boulders with underlying silt; frozen ground at bottom of depth profile</u>
<u>Taylor Nunatak</u>	<u>TN3-5</u>	<u>Valley floor; nearby snow patches; few glacial erratics; surface covered primarily by small boulders and cobbles with underlying silt</u>

Formatted: Left: 1", Right: 1", Top: 1", Bottom: 1".
Section start: New page, Width: 8.5", Height: 11"

819
820
821

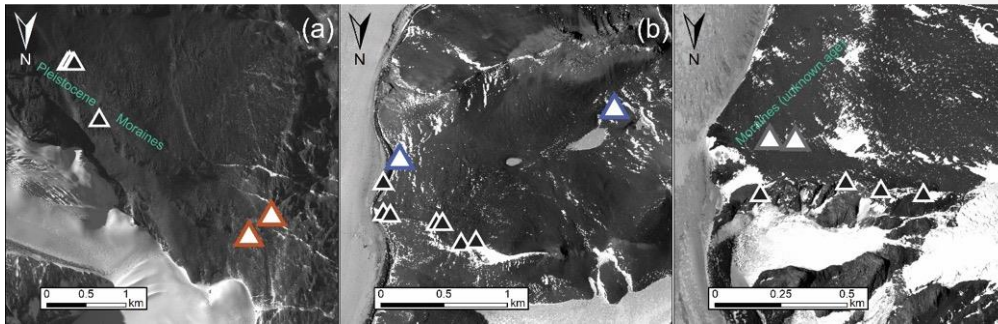
Formatted: Indent: First line: 0.5"
Formatted: Font: Not Bold

822 Figure 8: *In situ* exposure age measurements from glacial erratic boulders (black filled triangles)
823 (<http://antarctica.ice.d.org; Balco, 2020; Balter-Kennedy et al., 2020>) in relation to the meteoric ^{10}Be sample
824 locations from Roberts Massif (a, orange), Thanksgiving Valley (b, blue), and Mt. Franke (c, grey). Pleistocene age
825 moraines described by Balter-Kennedy et al. (2020) are labeled at Roberts Massif in green. We identified moraines
826 (green) of an unknown age at Mt. Franke.
827

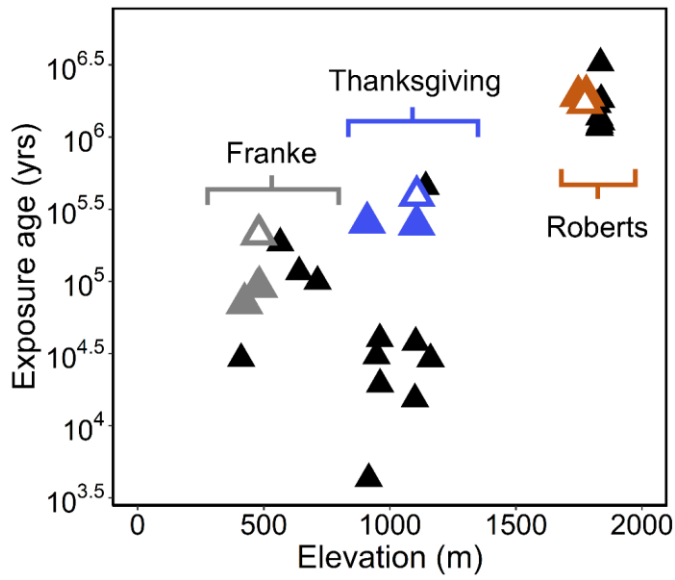
Field Code Changed

Formatted: Heading 2

828



829 **Figure 9:** Estimated (using NO_3^-) meteoric ^{10}Be exposure ages (open colored triangles) and inferred (using maximum
830 ^{10}Be concentration) exposure ages (closed colored triangles) without erosion compared to *in-situ* ages from ICE-D
831 (Balco, 2020) and Balter-Kennedy et al. (2020) (solid triangles) against elevation. All *in-situ* ages were measured from
832 glacial erratic boulders.
833

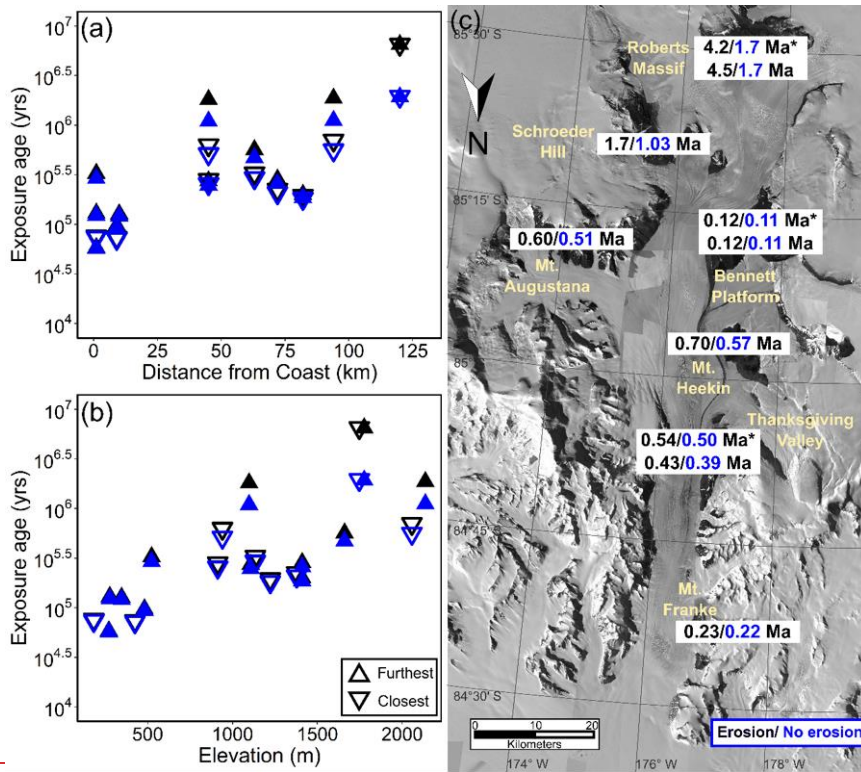


834

Formatted: Heading 2

Formatted: Heading 2, Left

835 **Figure 10:** Inferred surface exposure ages versus distance from the coast (a) and elevation (b), with (blue) and
 836 without (black) an assumed erosion term. Upward facing triangles are samples collected furthest from the glacier,
 837 while downward triangles are samples collected closest to the glacier. The estimated surface exposure ages using
 838 NO_3^- concentrations are included in panel (c). Values with asterisks (*) are ages calculated using the measured
 839 meteoric ^{10}Be concentrations in depth profiles.
 840



841

Formatted: Heading 2

Formatted: Heading 2, Left

842
843
844
845
846

Tables:

Table 1: Geographic data of samples collected from eleven ice-free areas along the Shackleton Glacier. Distance from the coast (aerial) was measured post-collection using ArcMap 10.3 software. Samples of the format "X-1" are samples collected furthest from the glacier in the transect.

Location	Sample name	Latitude	Longitude	Elevation (m)	Distance from coast (km)
Mt. Augustana	AV2-1	-85.1706	-174.1338	1410	72
Mt. Augustana	AV2-8	-85.1676	-174.1393	1378	72
Bennett Platform	BP2-1	-85.2121	-177.3576	1410	82
Bennett Platform	BP2-8	-85.2024	-177.3907	1222	82
Mt. Franke	MF2-1	-84.6236	-176.7353	480	9
Mt. Franke	MF2-4	-84.6237	-176.7252	424	9
Mt. Heekin	MH2-1	-85.0299	-177.2405	1660	63
Mt. Heekin	MH2-8	-85.0528	-177.4099	1134	63
Mt. Speed	MSP2-1	-84.4819	-176.5070	270	0
Mt. Speed	MSP2-4	-84.4811	-176.4864	181	0
Mt. Speed	MSP4-1	-84.4661	-177.1224	276	0
Mt. Wasco	MW4-1	-84.5600	-176.8177	345	10
Nilsen Peak	NP2-5	-84.6227	-176.7501	670	0
Roberts Massif	RM2-1	-85.4879	-177.1844	1776	120
Roberts Massif	RM2-8	-85.4857	-177.1549	1747	120
Schroeder Hill	SH3-2	-85.3597	-175.0693	2137	94
Schroeder Hill	SH3-8	-85.3569	-175.1621	2057	94
Thanksgiving Valley	TGV2-1	-84.9190	-177.0603	1107	45
Thanksgiving Valley	TGV2-8	-84.9145	-176.8860	912	45
Taylor Nunatak	TN3-1	-84.9227	-176.1242	1097	45
Taylor Nunatak	TN3-5	-84.9182	-176.1282	940	45

847
848

Formatted: Heading 2

Formatted: Heading 2

Formatted: Heading 2, Left

Formatted: Heading 2, Left

Formatted: Heading 2, Left

Formatted: Heading 2, Left

Formatted: Heading 2, Left

Formatted: Heading 2, Left

Formatted: Heading 2, Left

Formatted: Heading 2, Left

Formatted: Heading 2, Left

Formatted: Heading 2, Left

Formatted: Heading 2, Left

Formatted: Heading 2, Left

Formatted: Heading 2, Left

Formatted: Heading 2, Left

Formatted: Heading 2, Left

Formatted: Heading 2, Left

Formatted: Heading 2, Left

Formatted: Heading 2, Left

Formatted: Heading 2, Left

Formatted: Heading 2, Left

Formatted: Heading 2, Left

Formatted: Heading 2, Left

Formatted: Heading 2, Left

Formatted: Heading 2

849
850

Table 2: Surface features of the sample locations from the Shackleton Glacier region.

Location	Sample name	Sample description
Mt. Augustana	AV2-1	Up valley from Gallup Glacier (tributary glacier); at valley floor; surface covered by cobbles and pebbles; red-stained sandstones nearby; frozen ground at bottom of depth profile
Mt. Augustana	AV2-8	At toe of Gallup Glacier; surface covered primarily by boulders; mainly sand between boulders
Bennett Platform	BP2-1	On larger moraine; local depression between two boulder lines, up valley from McGregor Glacier (tributary glacier); at valley floor
Bennett Platform	BP2-8	At toe of McGregor Glacier (tributary glacier); surface covered primarily by boulders; mainly sand between boulders
Mt. Franke	MF2-1	Bottom of wide valley floor; near small moraine; frozen soil at bottom of depth profile
Mt. Franke	MF2-4	Bottom of wide valley floor; near small moraine
Mt. Heekin	MH2-1	On high elevation saddle; surface covered by sparse small boulders, cobbles, and pebbles; poorly consolidated till; frozen ground at bottom of profile
Mt. Heekin	MH2-8	At toe of Baldwin Glacier (alpine glacier) on valley floor; two ponds nearby; surface covered by loose rocks and sand; poorly consolidated till; possible polygonal surface nearby
Mt. Speed	MSP2-1	Steep slope; large granite boulders; scree
Mt. Speed	MSP2-4	Near cliff by Shackleton Glacier; large granite boulders; scree
Mt. Speed	MSP4-1	Spur on level with glacier; frozen soil near 5 cm depth
Mt. Wasko	MW4-1	Steep slope; large granite boulders; scree; nearby snowpack
Nilsen Peak	NP2-5	On ridge; near large snow patch
Roberts Massif	RM2-1	Near thin moraine; red-stained sandstones nearby with etches; frozen ground at bottom of depth profile
Roberts Massif	RM2-8	Near thin moraine and Sirius Group diamict; large boulders nearby with unconsolidated sediment
Schroeder Hill	SH3-2	Red-stained sandstone; poorly consolidated till; bedrock at bottom of profile
Schroeder Hill	SH3-8	Red-stained sandstone; poorly consolidated till;
Thanksgiving Valley	TGV2-1	Lightly uphill on valley wall; poorly consolidated till; frozen ground at bottom of depth profile; polygonal surface nearby
Thanksgiving Valley	TGV2-8	At the toe of Shackleton Glacier; near thin moraines, surface covered primarily large boulders
Taylor Nunatak	TN3-1	On ridge; surface covered by small boulders with underlying silt; frozen ground at bottom of depth profile
Taylor Nunatak	TN3-5	Valley floor; nearby snow patches; few glacial erratics; surface covered primarily by small boulders and cobbles with underlying silt

Formatted: Heading 2

Formatted: Heading 2, Left

Formatted: Heading 2, Left

Formatted: Heading 2, Left

Formatted: Heading 2, Left

Formatted: Heading 2, Left

Formatted: Heading 2, Left

Formatted: Heading 2, Left

Formatted: Heading 2, Left

Formatted: Heading 2, Left

Formatted: Heading 2, Left

Formatted: Heading 2, Left

Formatted: Heading 2, Left

Formatted: Heading 2, Left

Formatted: Heading 2, Left

Formatted: Heading 2, Left

Formatted: Heading 2, Left

Formatted: Heading 2, Left

Formatted: Heading 2, Left

Formatted: Heading 2, Left

Formatted: Heading 2, Left

Formatted: Heading 2, Left

Formatted: Heading 2, Left

Formatted: Heading 2, Left

Formatted: Heading 2, Left

Formatted: Heading 2, Left

Formatted: Heading 2

851

FGV2-1-0-5	0.498	398. ₂	151140	1.860	2.431	1.859	2.431	0.993	1.299
FGV2-1-5-10	0.500	398. ₂	151141	1.731	1.589	1.731	1.589	0.921	0.846
FGV2-1-10-15	0.497	393. ₃	151142	1.635	1.377	1.634	1.377	0.864	0.728
FGV2-1-15-20	0.502	399. ₂	151143	1.645	1.776	1.645	1.777	0.874	0.944
FGV2-1-20-25	0.498	403. ₂	151144	1.711	0.852	1.710	0.852	0.925	0.461
FGV2-1-25-30	0.497	399. ₂	151145	2.148	2.071	2.147	2.071	1.152	1.112
FGV2-8	0.499	399. ₂	151146	2.106	2.185	2.105	2.185	1.125	1.168
TN3-1	0.500	401. ₂	151562	7.092	5.903	7.091	5.903	3.802	3.165
TN3-5	0.500	401. ₂	151563	3.926	5.694	3.925	5.694	2.105	3.053

⁹Be was added through commercial SPEX carrier with a concentration of 1000 µg mL⁻¹.

**Isotopic analysis was conducted at PRIME Laboratory; ratios were normalized against standard 07KNSTD3110 with an assumed ratio of 2850×10^{-15} (Nishizumi et al., 2007). Blank ¹⁰Be/⁹Be ratio values averaged $8.152 \pm 1.884 \times 10^{-15}$.

856
857
858

Table 4: Exposure ages calculated from Eq. (1-6) and estimated ages using NO₃⁻ concentration data.

Location	Measured inventory (10 ¹¹ atoms)	Measured exposure age with <i>E</i> (Ma)	Measured exposure age without <i>E</i> (Ma)	Estimated inventory (10 ¹¹ atoms)*	Estimated exposure age with <i>E</i> (Ma)*	Estimated exposure age without <i>E</i> (Ma)*
Augustana	-	-	-	0.580	0.601	0.505
Bennett	0.135	0.115	0.106	0.143	0.122	0.113
Franke	-	-	-	0.268	0.232	0.217
Heekin	-	-	-	0.646	0.703	0.571
Roberts	1.47	4.15	1.67	1.51	4.54	1.74
Schroeder	-	-	-	1.05	1.66	1.03
Thanksgiving	0.570	0.535	0.495	0.465	0.426	0.394

*Estimations derived from linear relationship between NO₃⁻ concentration and meteoric 10Be concentration

859

860 **Table-Table 35:** Estimated exposure ages-durations using relationship between maximum ¹⁰Be concentration and
 861 inventory in Figure S4-7 (Graly et al., 2010)(Bierman et al., 2014).
 862

Sample name	<u>Measured inventory (10¹¹ atoms)</u>	Inferred inventory (10 ¹¹ atoms)	<u>Inferred exposure age duration with <i>E</i> (Ma)</u>	<u>Inferred exposure age duration without <i>E</i> (Ma)</u>
AV2-1		0.38	0.285	0.258
AV2-8		0.33	0.224	0.207
BP2-1	<u>0.135</u>	0.31	0.200	0.186
BP2-8		0.31	0.195	0.181
MF2-1		0.21	0.097	0.094
MF2-4		0.18	0.074	0.072
MH2-1		0.59	0.565	0.469
MH2-8		0.42	0.328	0.292
MSP2-1		0.16	0.058	0.057
MSP2-4		0.18	0.076	0.074
MSP4-1		0.24	0.129	0.123
MW4-1		0.24	0.127	0.121
NP2-5		0.42	0.326	0.291
RM2-1	<u>1.47</u>	1.24	>6.5*	1.93
RM2-8		1.50	>6.5*	1.94
SH3-2		1.07	1.87	1.11
SH3-8		0.67	0.702	0.560
TGV2-1	<u>0.535</u>	0.34	0.274	0.248
TGV2-8		0.38	0.282	0.255
TN3-1		1.06	1.81	1.09
TN3-5		0.62	0.628	0.512

*Outside of model range

Formatted Table

863

864

- 865 **References**
- 866 Ackert, R. P. and Kurz, M. D.: Age and uplift rates of Sirius Group sediments in the Dominion Range, Antarctica,
867 from surface exposure dating and geomorphology, *Glob. Planet. Change*, 42(1–4), 207–225,
868 doi:10.1016/j.gloplacha.2004.02.001, 2004.
- 869 Anderson, J. B., Shipp, S. S., Lowe, A. L., Wellner, J. S. and Mosola, A. B.: The Antarctic Ice Sheet during the Last
870 Glacial Maximum and its subsequent retreat history: a review, *Quat. Sci. Rev.*, 21, 49–70, doi:10.1016/S0277-
871 3791(01)00083-X, 2002.
- 872 Augustin, L., Barbante, C., Barnes, P. R. F., Barnola, J. M., Bigler, M., Castellano, E., Cattani, O., Chappellaz, J.,
873 Dahl-Jensen, D., Delmonte, B., Dreyfus, G., Durand, G., Falourd, S., Fischer, H., Flückiger, J., Hansson, M. E.,
874 Huybrechts, P., Jugie, G., Johnsen, S. J., Jouzel, J., Kaufmann, P., Kipfstuhl, J., Lambert, F., Lipenkov, V. Y., Littot,
875 G. C., Longinelli, A., Lorrain, R., Maggi, V., Masson-Delmotte, V., Miller, H., Mulvaney, R., Oerlemans, J., Oerter,
876 H., Orombelli, G., Parrenin, F., Peel, D. A., Petit, J. R., Raynaud, D., Ritz, C., Ruth, U., Schwander, J., Siegenthaler,
877 U., Souchez, R., Stauffer, B., Steffensen, J. P., Stenni, B., Stocker, T. F., Tabacco, I. E., Udisti, R., van de Wal, R. S.
878 W., van den Broeke, M., Weiss, J., Wilhelms, F., Winther, J. G., Wolff, E. W. and Zucchelli, M.: Eight glacial
879 cycles from an Antarctic ice core, *Nature*, 429(6992), 623–628, doi:10.1038/nature02599, 2004.
- 880 Balter-Kennedy, A., Bromley, G., Balco, G., Thomas, H. and Jackson, M. S.: A 14.5-million-year record of East
881 Antarctic Ice Sheet fluctuations from the central Transantarctic Mountains, constrained with cosmogenic ³He, ¹⁰Be,
882 ²¹Ne, and ²⁶Al, *Cryosph.*, 14(8), 2647–2672, doi:10.5194/tc-2020-57, 2020.
- 883 Barrett, P. J., Adams, C. J., McIntosh, W. C., Swisher, C. C. and Wilson, G. S.: Geochronological evidence
884 supporting Antarctic deglaciation three million years ago, *Nature*, 359, 816–818, 1992.
- 885 Bierman, P. R., Corbett, L. B., Graly, J. A., Neumann, T. A., Lini, A., Crosby, B. T. and Rood, D. H.: Preservation
886 of a Preglacial Landscape Under the Center of the Greenland Ice Sheet, *Science* (80-.), 344, 402–405,
887 doi:10.4159/harvard.9780674430501.c21, 2014.
- 888 Bockheim, J. G.: Landform and Soil Development in the McMurdo Dry Valleys, Antarctica: A Regional Synthesis,
889 *Arctic, Antarct. Alp. Res.*, 34(3), 308–317, doi:10.1080/15230430.2002.12003499, 2002.
- 890 Bromley, G. R. M., Hall, B. L., Stone, J. O., Conway, H. and Todd, C. E.: Late Cenozoic deposits at Reedy Glacier,
891 Transantarctic Mountains: implications for former thickness of the West Antarctic Ice Sheet, *Quat. Sci. Rev.*, 29(3–
892 4), 384–398, doi:10.1016/j.quascirev.2009.07.001, 2010.
- 893 Brown, E. T., Edmond, J. M., Raisbeck, G. M., Boursières, D. L., Yiou, F. and Measures, C. I.: Beryllium isotope
894 geochemistry in tropical river basins, *Geochim. Cosmochim. Acta*, 56(4), 1607–1624, doi:10.1016/0016-
895 7037(92)90228-B, 1992.
- 896 Cary, S. C., McDonald, I. R., Barrett, J. E. and Cowan, D. A.: On the rocks: The microbiology of Antarctic Dry
897 Valley soils, *Nat. Rev. Microbiol.*, 8(2), 129–138, doi:10.1038/nrmicro2281, 2010.
- 898 Claridge, G. G. C. and Campbell, I. B.: Origin of nitrate deposits., 1968a.
- 899 Claridge, G. G. C. and Campbell, I. B.: Soils of the Shackleton glacier region, Queen Maud Range, Antarctica, *New
900 Zeal. J. Sci.*, 11(2), 171–218, 1968b.
- 901 Claridge, G. G. C. and Campbell, I. B.: Salts in Antarctic soils, their distribution and relationship to soil processes,
902 *Soil Sci.*, 123(6), 377–384, 1977.
- 903 Clark, P. U., Dyke, A. S., Shakun, J. D., Carlson, A. E., Clark, J., Wohlfarth, B., Mitrovica, J. X., Hostetler, S. W.
904 and McCabe, A. M.: The Last Glacial Maximum, *Science* (80-.), 325, 710–714, doi:10.1126/science.1172873,
905 2009.
- 906 Collins, G. E., Hogg, I. D., Convey, P., Sancho, L. G., Cowan, D. A., Lyons, W. B., Adams, B. J., Wall, D. H. and
907 Green, T. G. A.: Genetic diversity of soil invertebrates corroborates timing estimates for past collapses of the West
908 Antarctic Ice Sheet, *Proc. Natl. Acad. Sci. U. S. A.*, 117(36), 22293–22302, doi:10.1073/pnas.2007925117, 2020.
- 909 Convey, P., Gibson, J. A. E., Hillenbrand, C. D., Hodgson, D. A., Pugh, P. J. A., Smellie, J. L. and Stevens, M. I.:

- 910 Antarctic terrestrial life - Challenging the history of the frozen continent?, *Biol. Rev.*, 83(2), 103–117,
911 doi:10.1111/j.1469-185X.2008.00034.x, 2008.
- 912 Diaz, M. A., Li, J., Michalski, G., Darrah, T. H., Adams, B. J., Wall, D. H., Hogg, I. D., Fierer, N., Welch, S. A.,
913 Gardner, C. B. and Lyons, W. B.: Stable isotopes of nitrate, sulfate, and carbonate in soils from the Transantarctic
914 Mountains, Antarctica: A record of atmospheric deposition and chemical weathering, *Front. Earth Sci.*, 8(341),
915 doi:10.3389/feart.2020.00341, 2020.
- 916 Dickinson, W. W., Schiller, M., Ditchburn, B. G., Graham, I. J. and Zondervan, A.: Meteoric Be-10 from Sirius
917 Group suggests high elevation McMurdo Dry Valleys permanently frozen since 6 Ma, *Earth Planet. Sci. Lett.*, 355–
918 356, 13–19, doi:10.1016/j.epsl.2012.09.003, 2012.
- 919 Ebert, K., Willenbring, J., Norton, K. P., Hall, A. and Hättestrand, C.: Meteoric ¹⁰Be concentrations from saprolite
920 and till in northern Sweden: Implications for glacial erosion and age, *Quat. Geochronol.*, 12, 11–22,
921 doi:10.1016/j.quageo.2012.05.005, 2012.
- 922 Elliot, D. H. and Fanning, C. M.: Detrital zircons from upper Permian and lower Triassic Victoria Group sandstones,
923 Shackleton Glacier region, Antarctica: Evidence for multiple sources along the Gondwana plate margin, *Gondwana
924 Res.*, 13, 259–274, doi:10.1016/j.gr.2007.05.003, 2008.
- 925 Elliot, D. H., Collinson, J. W. and Green, W. J.: Lakes in dry valleys at 85°S near Mount Heekin, Shackleton
926 Glacier, *Antarct. J. United States*, 31(2), 25–27, 1996.
- 927 Everett, K. R.: SOILS OF THE MESERVE GLACIER AREA, WRIGHT VALLEY, SOUTH VICTORIA LAND,
928 ANTARCTICA, *Soil Sci.*, 112(6), 425–438 [online] Available from: [https://oae.ovid.com/article/00010694-
929 197112000-00007/HTML](https://oae.ovid.com/article/00010694-197112000-00007/HTML) (Accessed 17 June 2021), 1971.
- 930 Fraser, C. I., Nikula, R., Ruzzante, D. E. and Waters, J. M.: Poleward bound: Biological impacts of Southern
931 Hemisphere glaciation, *Trends Ecol. Evol.*, 27(8), 462–471, doi:10.1016/j.tree.2012.04.011, 2012.
- 932 Frey, M. M., Savarino, J., Morin, S., Erbland, J. and Martins, J. M. F.: Photolysis imprint in the nitrate stable isotope
933 signal in snow and atmosphere of East Antarctica and implications for reactive nitrogen cycling., 2009.
- 934 Gasson, E., DeConto, R. M., Pollard, D. and Levy, R. H.: Dynamic Antarctic ice sheet during the early to mid-
935 Miocene, *Proc. Natl. Acad. Sci. U. S. A.*, 113(13), 3459–3464, doi:10.1073/pnas.1516130113, 2016.
- 936 Golledge, N. R., Fogwill, C. J., Mackintosh, A. N. and Buckley, K. M.: Dynamics of the last glacial maximum
937 Antarctic ice-sheet and its response to ocean forcing, *Proc. Natl. Acad. Sci. U. S. A.*, 109(40), 16052–16056,
938 doi:10.1073/pnas.1205385109, 2012.
- 939 Golledge, N. R., Levy, R. H., McKay, R. M., Fogwill, C. J., White, D. A., Graham, A. G. C., Smith, J. A.,
940 Hillenbrand, C. D., Licht, K. J., Denton, G. H., Ackert, R. P., Maas, S. M. and Hall, B. L.: Glaciology and
941 geological signature of the Last Glacial Maximum Antarctic ice sheet, *Quat. Sci. Rev.*, 78, 225–247,
942 doi:10.1016/j.quascirev.2013.08.011, 2013.
- 943 Graham, I., Ditchburn, R. G., Claridge, G. G. G., Whitehead, N. E., Zondervan, A. and Sheppard, D. S.: Dating
944 Antarctic soils using atmospheric derived ¹⁰Be and nitrate, *R. Soc. New Zeal. Bull.*, 35, 429–436, 2002.
- 945 Graham, I. J., Ditchburn, R. G., Sparks, R. J. and Whitehead, N. E.: ¹⁰Be investigations of sediments, soils and loess
946 at GNS, *Nucl. Instruments Methods Phys. Res. B*, 123, 307–318, 1997.
- 947 Graly, J. A., Bierman, P. R., Reusser, L. J. and Pavich, M. J.: Meteoric ¹⁰Be in soil profiles - A global meta-
948 analysis, *Geochim. Cosmochim. Acta*, 74, 6814–6829, doi:10.1016/j.gca.2010.08.036, 2010.
- 949 Graly, J. A., Licht, K. J., Druschel, G. K. and Kaplan, M. R.: Polar desert chronologies through quantitative
950 measurements of salt accumulation, *Geology*, 46(4), 351–354, doi:10.1130/G39650.1, 2018.
- 951 Gulick, S. P. S., Shevenell, A. E., Montelli, A., Fernandez, R., Smith, C., Warny, S., Bohaty, S. M., Sjunneskog, C.,
952 Leventer, A., Frederick, B. and Blankenship, D. D.: Initiation and long-term instability of the East Antarctic Ice
953 Sheet, *Nature*, 552(7684), 225–229, doi:10.1038/nature25026, 2017.

- 954 Hambrey, M. J., Webb, P. N., Harwood, D. M. and Krissek, L. A.: Neogene glacial record from the Sirius Group of
 955 the Shackleton Glacier region, central Transantarctic Mountains, Antarctica, *GSA Bull.*, 115(8), 994–1015,
 956 doi:10.1130/B25183.1, 2003.
- 957 Ivy-Ochs, S., Schluchter, C., Kubik, P. W., Dittrich-Hannen, B. and Beer, J.: Minimum 10Be exposure ages of early
 958 Pliocene for the Table Mountain plateau and the Sirius Group at Mount Fleming, Dry Valleys, Antarctica, *Geology*,
 959 23(11), 1007–1010, 1995.
- 960 Jackson, A., Davila, A. F., Böhlke, J. K., Sturchio, N. C., Sevanthi, R., Estrada, N., Brundrett, M., Lacelle, D.,
 961 McKay, C. P., Poghosyan, A., Pollard, W. and Zacny, K.: Deposition, accumulation, and alteration of Cl⁻, NO₃⁻,
 962 ClO₄⁻ and ClO₃⁻ salts in a hyper-arid polar environment: Mass balance and isotopic constraints, *Geochim.*
 963 *Cosmochim. Acta*, 182, 197–215, doi:10.1016/j.gca.2016.03.012, 2016.
- 964 Jones, R. S., Mackintosh, A. N., Norton, K. P., Gолledge, N. R., Fogwill, C. J., Kubik, P. W., Christl, M. and
 965 Greenwood, S. L.: Rapid Holocene thinning of an East Antarctic outlet glacier driven by marine ice sheet instability,
 966 *Nat. Commun.*, 6(8910), 9910, doi:10.1038/ncomms9910, 2015.
- 967 Kaplan, M. R., Licht, K. J., Winckler, G., Schaefer, J. M., Bader, N., Mathieson, C., Roberts, M., Kassab, C. M.,
 968 Schwartz, R. and Graly, J. A.: Middle to Late Pleistocene stability of the central East Antarctic Ice Sheet at the head
 969 of Law Glacier, *Geology*, 45(11), 963–966, doi:10.1130/G39189.1, 2017.
- 970 Korschinek, G., Bergmaier, A., Faestermann, T., Gerstmann, U. C., Knie, K., Rugel, G., Wallner, A., Dillmann, I.,
 971 Dollinger, G., von Gostomski, C. L., Kossert, K., Maiti, M., Poutivtsev, M. and Remmert, A.: A new value for the
 972 half-life of 10Be by Heavy-Ion Elastic Recoil Detection and liquid scintillation counting, *Nucl. Instruments*
 973 *Methods Phys. Res. Sect. B Beam Interact. with Mater. Atoms*, 268(2), 187–191, doi:10.1016/j.nimb.2009.09.020,
 974 2010.
- 975 Lewis, A. R., Marchant, D. R., Ashworth, A. C., Hedenäs, L., Hemming, S. R., Johnson, J. V., Leng, M. J.,
 976 Machlus, M. L., Newton, A. E., Raine, J. I., Willenbring, J. K., Williams, M. and Wolfe, A. P.: Mid-Miocene
 977 cooling and the extinction of tundra in continental Antarctica, *Proc. Natl. Acad. Sci. U. S. A.*, 105(31), 10676–
 978 10680, doi:10.1073/pnas.0802501105, 2008.
- 979 Lyons, W. B., Mayewski, P. A., Spencer, M. J. and Twickler, M. S.: Nitrate concentrations in snow from remote
 980 areas: implication for the global NO_x flux, *Biogeochemistry*, 9(3), 211–222, doi:10.1007/BF00000599, 1990.
- 981 Lyons, W. B., Deuerling, K., Welch, K. A., Welch, S. A., Michalski, G., Walters, W. W., Nielsen, U., Wall, D. H.,
 982 Hogg, I. and Adams, B. J.: The Soil Geochemistry in the Beardmore Glacier Region, Antarctica: Implications for
 983 Terrestrial Ecosystem History, *Sci. Rep.*, 6, 26189, doi:10.1038/srep26189, 2016.
- 984 Mackintosh, A., Gолledge, N., Domack, E., Dunbar, R., Leventer, A., White, D., Pollard, D., Deconto, R., Fink, D.,
 985 Zwartz, D., Gore, D. and Lavoie, C.: Retreat of the East Antarctic ice sheet during the last glacial termination, *Nat.*
 986 *Geosci.*, 4(3), 195–202, doi:10.1038/ngeo1061, 2011.
- 987 Mackintosh, A. N., Verleyen, E., O’Brien, P. E., White, D. A., Jones, R. S., McKay, R., Dunbar, R., Gore, D. B.,
 988 Fink, D., Post, A. L., Miura, H., Leventer, A., Goodwin, I., Hodgson, D. A., Lilly, K., Crosta, X., Gолledge, N. R.,
 989 Wagner, B., Berg, S., van Ommen, T., Zwartz, D., Roberts, S. J., Vyverman, W. and Masse, G.: Retreat history of
 990 the East Antarctic Ice Sheet since the Last Glacial Maximum, *Quat. Sci. Rev.*, 100, 10–30,
 991 doi:10.1016/j.quascirev.2013.07.024, 2014.
- 992 Marchant, D. R., Denton, G. H., Swisher, C. C. and Potter, N.: Late Cenozoic Antarctic paleoclimate reconstructed
 993 from volcanic ashes in the Dry Valleys region of southern Victoria Land, *Geol. Soc. Am. Bull.*, 108(2), 181–194,
 994 doi:https://doi.org/10.1130/0016-7606(1996)108%3C0181:LCAPRF%3E2.3.CO;2, 1996.
- 995 McHargue, L. R. and Damon, P. E.: The global beryllium 10 cycle, *Rev. Geophys.*, 29(2), 141–158,
 996 doi:10.1029/91RG00072, 1991.
- 997 Menzies, J., van der Meer, J. J. M. and Rose, J.: Till-as a glacial “tectomict”, its internal architecture, and the
 998 development of a “typing” method for till differentiation, *Geomorphology*, 75, 172–200,
 999 doi:10.1016/j.geomorph.2004.02.017, 2006.

- 1000 Michalski, G., Bockheim, J. G., Kendall, C. and Thiemens, M.: Isotopic composition of Antarctic Dry Valley
1001 nitrate: Implications for NO_y sources and cycling in Antarctica, *Geophys. Res. Lett.*, 32(13), 1–4,
1002 doi:10.1029/2004GL022121, 2005.
- 1003 Morgan, D., Putkonen, J., Balco, G. and Stone, J.: Quantifying regolith erosion rates with cosmogenic nuclides ¹⁰
1004 Be and ²⁶Al in the McMurdo Dry Valleys, Antarctica, *J. Geophys. Res.*, 115, F03037, doi:10.1029/2009JF001443,
1005 2010.
- 1006 Nishiizumi, K., Imamura, M., Caffee, M. W., Southon, J. R., Finkel, R. C. and McAninch, J.: Absolute calibration of
1007 ¹⁰Be AMS standards, *Nucl. Instruments Methods Phys. Res. B*, 258, 403–413, doi:10.1016/j.nimb.2007.01.297,
1008 2007.
- 1009 Paulsen, T. S., Encarnación, J. and Grunow, A. M.: Structure and timing of transpressional deformation in the
1010 Shackleton Glacier area, Ross orogen, Antarctica, *J. Geol. Soc. London.*, 161(6), 1027–1038, doi:10.1144/0016-
1011 764903-040, 2004.
- 1012 Pavich, M. J., Brown, L., Klein, J. and Middleton, R.: ¹⁰Be accumulation in a soil chronosequence, *Earth Planet.*
1013 *Sci. Lett.*, 68, 198–204, doi:10.1016/0012-821X(84)90151-1, 1984.
- 1014 Pavich, M. J., Brown, L., Harden, J., Klein, J. and Middleton, R.: ¹⁰Be distribution in soils from Merced River
1015 terraces, California, *Geochim. Cosmochim. Acta*, 50, 1727–1735, doi:10.1016/0016-7037(86)90134-1, 1986.
- 1016 Pollard, D. and DeConto, R. M.: Modelling West Antarctic ice sheet growth and collapse through the past five
1017 million years, *Nature*, 458(7236), 329–332, doi:10.1038/nature07809, 2009.
- 1018 Reich, M. and Bao, H.: Nitrate deposits of the Atacama Desert: A marker of long-term hyperaridity, *Elements*,
1019 14(4), 251–256, doi:10.2138/gselements.14.4.251, 2018.
- 1020 Scarrow, J. W., Balks, M. R. and Almond, P. C.: Three soil chronosequences in recessional glacial deposits near the
1021 polar plateau, in the Central Transantarctic Mountains, Antarctica, *Antarct. Sci.*, 26(5), 573–583,
1022 doi:10.1017/S0954102014000078, 2014.
- 1023 Scherer, R. P., DeConto, R. M., Pollard, D. and Alley, R. B.: Windblown Pliocene diatoms and East Antarctic Ice
1024 Sheet retreat, *Nat. Commun.*, 7(1), 1–9, doi:10.1038/ncomms12957, 2016.
- 1025 Schiller, M., Dickinson, W., Ditchburn, R. G., Graham, I. J. and Zondervan, A.: Atmospheric ¹⁰Be in an Antarctic
1026 soil: Implications for climate change, *J. Geophys. Res.*, 114(F1), 1–8, doi:10.1029/2008jf001052, 2009.
- 1027 Spector, P. and Balco, G.: Exposure-age data from across Antarctica reveal mid-Miocene establishment of polar
1028 desert climate, *Geol. Soc. Am. | Geol.*, 1, doi:10.1130/G47783.1, 2020.
- 1029 Spector, P., Stone, J., Cowdery, S. G., Hall, B., Conway, H. and Bromley, G.: Rapid early-Holocene deglaciation in
1030 the Ross Sea, Antarctica, *Geophys. Res. Lett.*, 44(15), 7817–7825, doi:10.1002/2017GL074216, 2017.
- 1031 Steig, E., Stuiver, M. and Polissar, P.: Cosmogenic isotope concentrations at Taylor Dome, Antarctica, *Antarct. J.*
1032 *United States*, 30, 95–97, 1995.
- 1033 Stevens, M. I. and Hogg, I. D.: Long-term isolation and recent range expansion from glacial refugia revealed for the
1034 endemic springtail *Gomphiocephalus hodgsoni* from Victoria Land, Antarctica, *Mol. Ecol.*, 12(9), 2357–2369,
1035 doi:10.1046/j.1365-294X.2003.01907.x, 2003.
- 1036 Stone, J.: A rapid fusion method for separation of beryllium-10 from soils and silicates, *Geochim. Cosmochim.*
1037 *Acta*, 62(3), 555–561, doi:10.1016/S0016-7037(97)00340-2, 1998.
- 1038 Stroeven, A. P., Prentice, M. L. and Kleman, J.: On marine microfossil transport and pathways in Antarctica during
1039 the late Neogene: Evidence from the Sirius Group at Mount Fleming, *Geology*, 24(8), 727–730, doi:10.1130/0091-
1040 7613(1996)024<0727:ommtap>2.3.co;2, 1996.
- 1041 Talarico, F. M., McKay, R. M., Powell, R. D., Sandroni, S. and Naish, T.: Late Cenozoic oscillations of Antarctic
1042 ice sheets revealed by provenance of basement clasts and grain detrital modes in ANDRILL core AND-1B, *Glob.*
1043 *Planet. Change*, 96–97, 23–40, doi:10.1016/j.gloplacha.2009.12.002, 2012.

- 1044 Valletta, R. D., Willenbring, J. K., Lewis, A. R., Ashworth, A. C. and Caffee, M.: Extreme decay of meteoric
1045 beryllium-10 as a proxy for persistent aridity, *Sci. Rep.*, 5, 17813, doi:10.1038/srep17813, 2015.
- 1046 Webb, P. N. and Harwood, D. M.: Late Cenozoic glacial history of the Ross embayment, Antarctica, *Quat. Sci.*
1047 *Rev.*, 10(2–3), 215–223, doi:10.1016/0277-3791(91)90020-U, 1991.
- 1048 Webb, P. N., Harwood, D. M., McKelvey, B. C., Mercer, J. H. and Stott, L. D.: Cenozoic marine sedimentation and
1049 ice-volume variation on the East Antarctic craton, *Geology*, 12(5), 287–291, doi:10.1130/0091-
1050 7613(1984)12<287:cmsaiv>2.0.co;2, 1984.
- 1051 Webb, P. N., Harwood, D. M., Mabin, M. G. C. and McKelvey, B. C.: A marine and terrestrial Sirius Group
1052 succession, middle Beardmore Glacier-Queen Alexandra Range, Transantarctic Mountains, Antarctica, *Mar.*
1053 *Micropaleontol.*, 27(1–4), 273–297, doi:10.1016/0377-8398(95)00066-6, 1996.
- 1054 Welch, K. A., Lyons, W. B., Whisner, C., Gardner, C. B., Gooseff, M. N., Mcknight, D. M. and Prisco, J. C.: Spatial
1055 variations in the geochemistry of glacial meltwater streams in the Taylor Valley, Antarctica, *Antarct. Sci.*, 22(6),
1056 662–672, doi:10.1017/S0954102010000702, 2010.
- 1057 Willenbring, J. K. and von Blanckenburg, F.: Meteoric cosmogenic Beryllium-10 adsorbed to river sediment and
1058 soil: Applications for Earth-surface dynamics, *Earth-Science Rev.*, 98(1–2), 105–122,
1059 doi:10.1016/j.earscirev.2009.10.008, 2010.
- 1060 You, C. F., Lee, T. and Li, Y. H.: The partition of Be between soil and water, *Chem. Geol.*, 77(2), 105–118,
1061 doi:10.1016/0009-2541(89)90136-8, 1989.
- 1062